



Influence of salt-related mechanical layering on the seismic potential of active faults: Insights from the southwestern Valencia Trough (W Mediterranean)

Iván Martín-Rojas¹, Adrià Ramos^{2,1}, Menno De Ruig³, Iván Medina-Cascales¹, Eva Santamaría-Pérez¹, and Pedro Alfaro¹

¹Dpto. de Ciencias de la Tierra y del Medio Ambiente, Universidad de Alicante, Campus San Vicente s/n, 03690, San Vicente del Raspeig, Alicante, Spain

²Departament de Botànica i Geologia, Universitat de València, 46010 Burjassot, Valencia, Spain

³Lithologic, 2582 LD The Hague, the Netherlands

Correspondence: Iván Martín-Rojas (ivan.martin@ua.es)

Received: 14 April 2025 – Discussion started: 14 May 2025

Revised: 24 November 2025 – Accepted: 27 March 2026 – Published: 12 May 2026

Abstract. We present a structural and seismotectonic analysis of active faults in the southwestern Valencia Trough (western Mediterranean) on the basis of subsurface datasets. In our study, we identify and characterise three major active faults: the Cullera Fault, with long-term slip rates that vary over time between 0.15 ± 0.1 and 0.4 ± 0.1 mm yr⁻¹; the oblique Albufera Fault, with a long-term slip rate of 0.2 ± 0.1 mm yr⁻¹; and the normal Valencia Fault.

The seismogenic character of the southwestern Valencia Trough is controlled by a mechanically weak layer consisting of Triassic evaporites. This weak layer induces partial-to-complete decoupling between the suprasalt and subsalt successions, leading to two distinct mechanisms driving fault displacement: tectonic activity and salt withdrawal. A quantitative evolutionary analysis of the Cullera Fault reveals that these two mechanisms occur alternately over time.

The presence of a mechanically weak layer has implications for seismicity. Earthquakes can nucleate within both sub- and suprasalt successions, with total or partial decoupling influencing rupture propagation. We discuss how these two scenarios lead to different earthquakes and thus impact the seismic hazard of a region. Empirical source-scaling relationships, which are commonly used to estimate the seismogenic potential of active faults, generally assume a homogeneous seismogenic crust. To address this limitation, we propose a methodological approach based on the use of the aspect ratio. Using this method, the maximum magnitudes for

suprasalt ruptures are 5.8–6.4, 5.4–6.2, and 5.1–5.9 for the Cullera, Valencia, and Albufera faults, respectively. These values are 11 %–25 % lower than those obtained by considering the rupture of the entire seismogenic crust. Our findings highlight the need to incorporate stratigraphic mechanical layering into seismic hazard assessments, particularly in salt-influenced tectonic settings.

1 Introduction

Seismic hazard analyses are often performed by scaling relationships. These relationships are regressions in which the seismogenic potential of active faults is derived from geometric parameters of the fault, such as the potential fault rupture length or area (Stirling et al., 2013). Pioneering works on scaling relationships began in the 1970s (Kanamori and Anderson, 1975; Geller, 1976). The regressions of Wells and Coppersmith (1994) represent a milestone in the application of scaling relationships, as they included a very large dataset of historical earthquakes. The equations proposed by Wells and Coppersmith became a standard for determining the seismogenic potential of active faults. Subsequently, other scaling relationships have been proposed, accounting for factors such as the tectonic environment, fault dip, or seismogenic thickness (Stirling et al., 2002 and 2013; Leonard, 2010, 2014; Huang et al., 2024; among many others).

Most scaling relationships employed to evaluate crustal earthquakes correlate the moment magnitude (M_w) with the fault dimensions (length, width, and/or area). Some of these scaling relationships consider the fault width vs. fault dip growth of ruptures for large earthquakes, as rupture width is limited by the maximum depth of the seismogenic crust (Leonard, 2010; Yen and Ma, 2011; Leonard, 2014; Cheng et al., 2019). Standard relationships include data from hundreds or even thousands of events. Therefore, the influence in these relationships of potential mechanical heterogeneities within the seismogenic crust should be implicit. However, because of the large amount of data, the mean regressions average out the less common situations, as the presence of a mechanical weak layer. Therefore, as a consequence of this averaging, the empirical relationships do not permit to compute the influence of potential heterogeneities within the seismogenic crust. These heterogeneities could control the vertical propagation of ruptures and, therefore, the magnitude of earthquakes.

Here, we present an analysis of several subsurface datasets, including high-resolution seismic profiles, from the southwestern Valencia Trough. We identify and characterise the main active faults in this region, and we carry out a detailed geometric description. The results of this analysis also emphasize that this region is characterised by a mechanically weak layer within the seismogenic crust. After mapping the main faults, we apply conventional scaling relationships to evaluate the potential magnitudes of future earthquakes. We propose a methodological approach for integrating the effects of mechanically weak layers – such as Triassic evaporites – into routine seismic hazard assessments, highlighting the need to refine existing scaling relationships in tectonically complex settings.

2 Tectonic setting

The Valencia Trough is an extensional basin located in the western Mediterranean region (Fig. 1). This basin is the result of polyphase tectonic evolution spanning from the Triassic to the present day, as it is located between the Betic–Balearic fold-and-thrust belt to the south, the Iberian Chain to the west, and the Catalan Coastal Range to the north (De Ruig, 1992; Guimerà and Álvaro, 1990; Maillard and Mauffret, 1999; Roca and Desegaulx, 1992; Roca et al., 2004; Vergés and Fernández, 2012). The tectonic evolution of the Valencia Trough is also partially influenced by extension related to the retreat of the Maghrebian–Ligurian Tethys subduction slab (Etheve et al., 2016; Faccenna et al., 2004; Jolivet and Faccenna, 2000; Maillard and Mauffret, 1999; Rehault et al., 1984; Roca et al., 1999; Séranne, 1999; van Hinsbergen et al., 2014).

The Valencia Trough (Fig. 1) underwent a Mesozoic rifting process related to the Iberian intraplate rift and the opening of the Western Tethys (Arche and López-Gómez, 1996;

Nebot and Guimerà, 2018; Ramos et al., 2023; Salas et al., 2001). This process led to the formation of NW–SE and NE–SW high-angle faults offsetting the pre-Mesozoic basement and to the deposition of a 5–15 km-thick Upper Jurassic–Lower Cretaceous succession.

During the Late Cretaceous, the onset of convergence between Nubia and Eurasia caused the transition from a Mesozoic extensional tectonic regime to successive compressional and extensional stages (Roca, 2001; Salas et al., 2001; Vergés and Sàbat, 1999). From the late Eocene to the Oligocene, the Valencia Trough was dominated by shortening. Onshore, this episode led to the formation of the intraplate Iberian Chain and Catalan Coastal Ranges (Gaspar-Escribano et al., 2004; Geel, 1995; Guimerà and Álvaro, 1990).

From the late Oligocene to the middle Miocene, the western Mediterranean region was subsequently affected by an extensional regime, driven by the complex interplay between the European–Cenozoic rift system (e.g., Séranne, 1999) and the rollback of the Maghrebian–Ligurian Tethys slab (Faccenna et al., 2004; van Hinsbergen et al., 2014). This extensional phase led to the formation of the Liguro-Provençal and Algerian Basins, as well as the Valencia Trough. However, subsidence in the southwestern Valencia Trough during this period cannot be accounted for by rifting, due to the limited occurrence of Cenozoic basement extensional faults (Roca and Guimerà, 1992). Therefore, extension has been interpreted as due to the collapse of a back-arc transient uplift event (Fang et al., 2021).

The extension in the Valencia Trough occurred immediately before or synchronously with the formation of the compressional Betic Cordillera. This compressional deformation is well expressed by a thin-skinned fold-and-thrust system observed in the Eastern Betic Cordillera (De Ruig, 1995; Sàbat et al., 2011) and in the Balearic Promontory (Mallorca and Ibiza Islands). At the same time, significant magmatic activity took place in the area. This magmatism was divided into two phases: (1) late Oligocene to Serravallian calc-alkaline activity and (2) Tortonian to present alkaline volcanic activity (Martí et al., 1992).

From the Pliocene to the present, the tectonic setting in the Valencia Trough has been dominated by NE–SW extension, as indicated by focal mechanisms (Stich et al., 2010) and broad regional global navigation satellite system (GNSS) analyses (Stich et al., 2006). This extension has been related to thermal subsidence (Roca, 1992, 1996, 2001; Roca and Guimerà, 1992; Roca et al., 1999; Gaspar-Escribano et al., 2004) and has been interpreted as the final stage of an aborted rift event responsible for the ENE motion of the Balearic promontory (Palano et al., 2015). Several normal active faults have been defined in the southwestern Valencia Trough thus far (Fig. 1): the Western Cabo Cullera Fault, Central-Western Cabo Cullera Fault, Central-Eastern Cabo Cullera Fault, Eastern Cabo Cullera Fault and Southwest Columbrete Fault (Perea, 2006). Some of these faults were previously recognised from vintage seismic lines (Díaz del

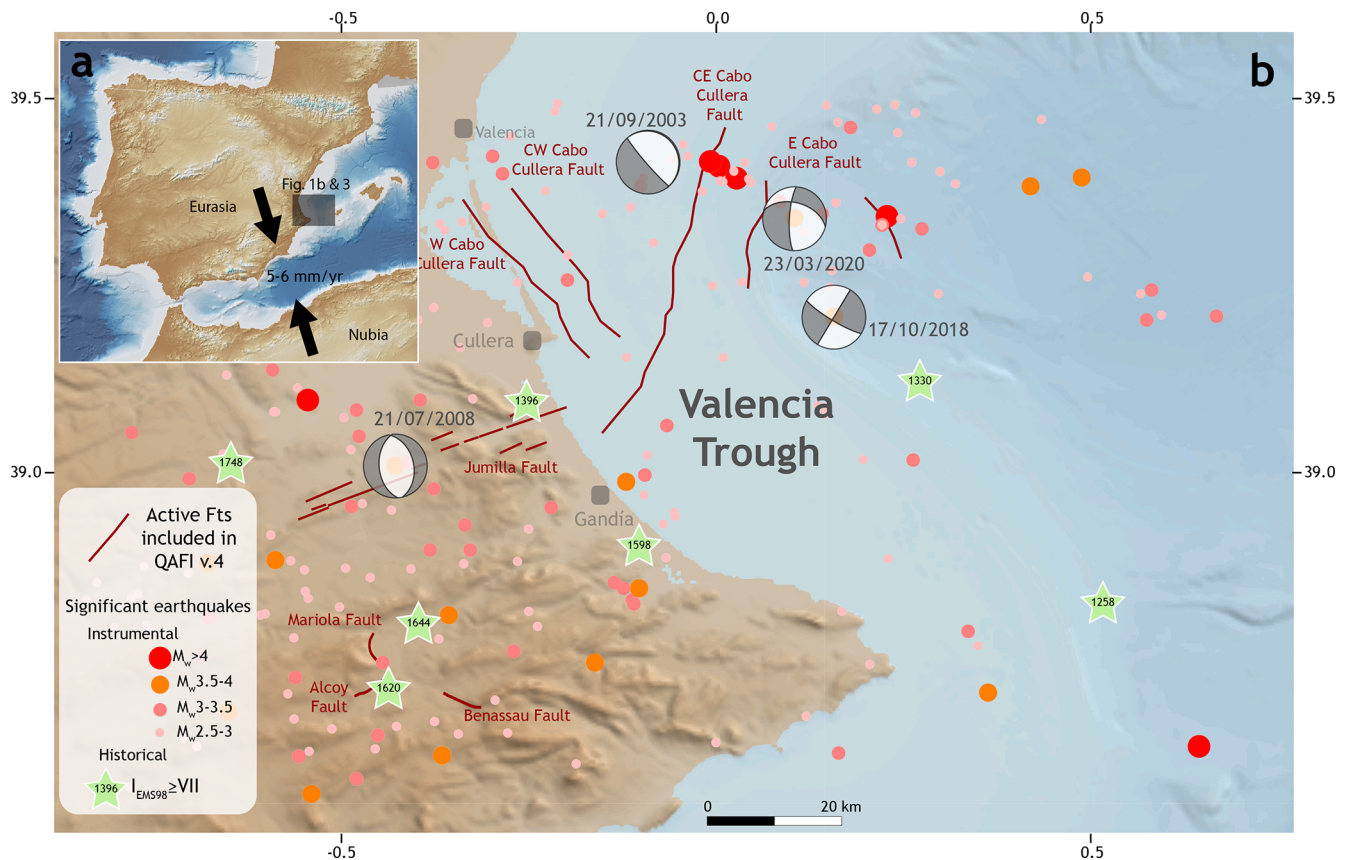


Figure 1. (a) Location of the Valencia Trough. Convergence vectors between Nubia and Eurasia are after DeMets et al. (1994), McClusky et al. (2003), Nocquet (2012), Nocquet and Calais (2003), Pérez-Peña et al. (2010), Serpelloni et al. (2007), and Stich et al. (2006). (b) Seismotectonic map of the southwestern Valencia Trough and surrounding areas. Fault traces from Quaternary-Active Faults of Iberia database (García-Mayordomo et al., 2012).

Rio et al., 1986; Roca, 1992, 1996; Perea, 2006; Maillard and Mauffret, 2013), but fault traces and geometry were defined only very approximately. Similarly, the slip rates derived from the displacement of Plio-Quaternary seismic reflectors observed in the vintage seismic lines present high uncertainties ($0.02 \pm 0.01 \text{ mm yr}^{-1}$; Perea, 2006). In the Valencia Trough, seismicity is characterised by low- to moderate-magnitude events (Fig. 1). The few available focal mechanisms (Stich et al., 2010; IGN, 2025) indicate a normal-oblique or strike slip kinematics, although these focal mechanisms present high uncertainties, mainly because they occur at long distances from seismic stations and are registered with significant azimuthal gaps (González, 2017). According to the data published by the Spanish Earthquake Catalogue (IGN, 2025), this seismicity is very shallow, as most of the events are assigned depths of less than 10 km (Fig. 2). However, these data should be taken with caution, as the depths assigned to these earthquakes present high uncertainties (González, 2017).

In the onshore domain located west of the Valencia Trough, only one major active structure, namely, the Jumilla

Fault, has been postulated (García-Mayordomo et al., 2012), together with other minor active faults (Alcoy, Mariola, and Benasau Faults). In this onshore area, several significant historical earthquakes have occurred, such as the 1396 Tavernes ($I_{EMS98} = \text{VIII-IX}$), 1620 Alcoy ($I_{EMS98} = \text{VIII-IX}$), 1644 Muro ($I_{EMS98} = \text{V}$) and 1748 Estubeny ($I_{EMS98} = \text{IX}$) earthquakes (Martínez-Solares and Mezcuca, 2002; IGN, 2025; Buform et al., 2015; Buform and Udías, 2022).

3 Data

The interpretation of the offshore area is based on mainly 2D multichannel seismic reflection data calibrated with well data (Fig. 3). The central part of the study area is covered by a high-quality seismic survey acquired by Fugro-Geoteam with the RV Geo Baltic, processed by Robertson Research International Ltd. in 2002. The survey consists of 30 seismic sections with an average length of 90 km (totalling approximately 2800 km). They are oriented WNW-ESE and NNE-SSW, with maximum spacings of 13 and 6 km, respectively. The details regarding the acquisition and processing param-

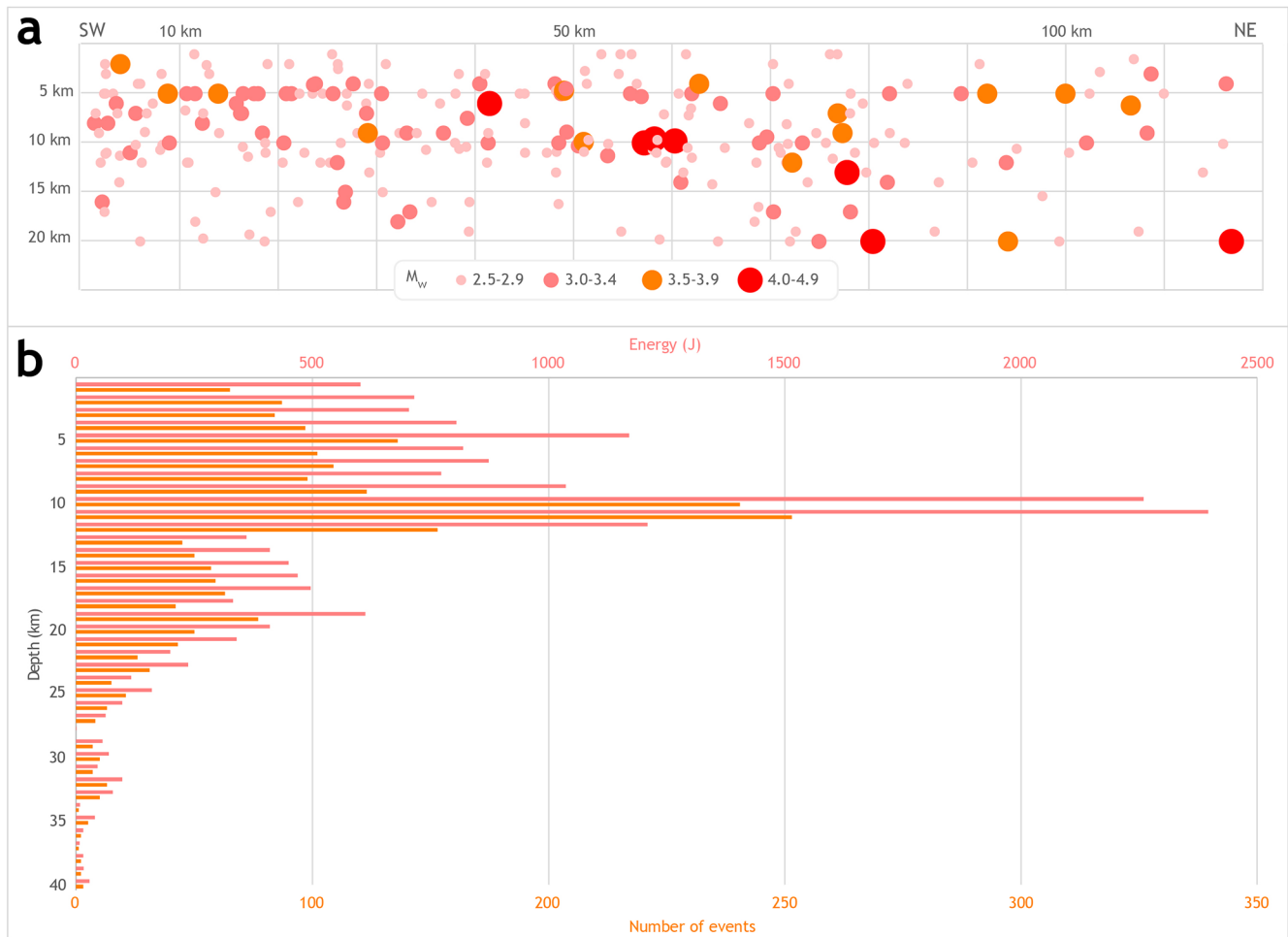


Figure 2. Seismicity of $M_w > 2.5$ in the southwestern Valencia Trough shallower than 20 km since 1950 from the *Instituto Geográfico Nacional* database (IGN, 2025). **(a)** Distribution of the depth of seismicity. The horizontal axis represents distance along the southwestern Valencia Trough in a SW-NE direction (from the SW shoreline to the NE Mediterranean Sea). **(b)** Energy (from magnitude) and depth histogram. In both graphics events with 0 km of the assigned depth are not represented (fixed depth).

eters can be found in Cameselle and Urgeles (2017). Most of the area affected by Plio-Quaternary faulting nearer to the coast is covered only by vintage 2D seismic lines from the late 1970s, acquired by various operators, which are publicly available upon request in the Instituto Geológico y Minero de España (IGME-CSIC) (<http://info.igme.es/sigeof/>, last access: 15 March 2025). More than 100 of these seismic lines, with a total line length of approximately 2500 km, were selected for mapping; although the quality of these lines varies from moderate to poor, the high-density grid spacing (varying from 1 to 3.5 km) allows fault mapping with reasonable confidence. The seismic interpretation was performed in two-way travel time (TWT) by using Move software (by Petex). The seismic dataset was converted to depths using velocity data derived from the Expanded Spread Profile (ESP) 7 (Pascal et al., 1992; Torné et al., 1992). A second-order polynomial trend was applied to establish time-depth relationships,

ensuring strong correlation with the well data, similar to the methodologies of Fang et al. (2021).

The interpretation of seismic horizons is calibrated by 9 offshore petroleum exploration wells, all of which penetrate the entire Neogene section and whose bottoms are in Mesozoic rocks. Original well reports, log data (lithology, dipmeter, gamma-ray, sonic and resistivity data) and palaeontological data (from cuttings and sidewall cores) were retrieved from the IGME-CSIC archive (<https://info.igme.es/hidrocarburos/>, last access: 15 March 2025). Well-to-seismic ties were established by integrating the sonic logs and using synthetic seismograms from end-of-well reports. Palaeontological analyses and range charts from the original well reports were reviewed and adapted to the Mediterranean biozonation of Lirer et al. (2019) to obtain approximate absolute ages for the seismic horizons.

No seismic data were available for the onshore area of southern Valencia and only two deep exploration wells were

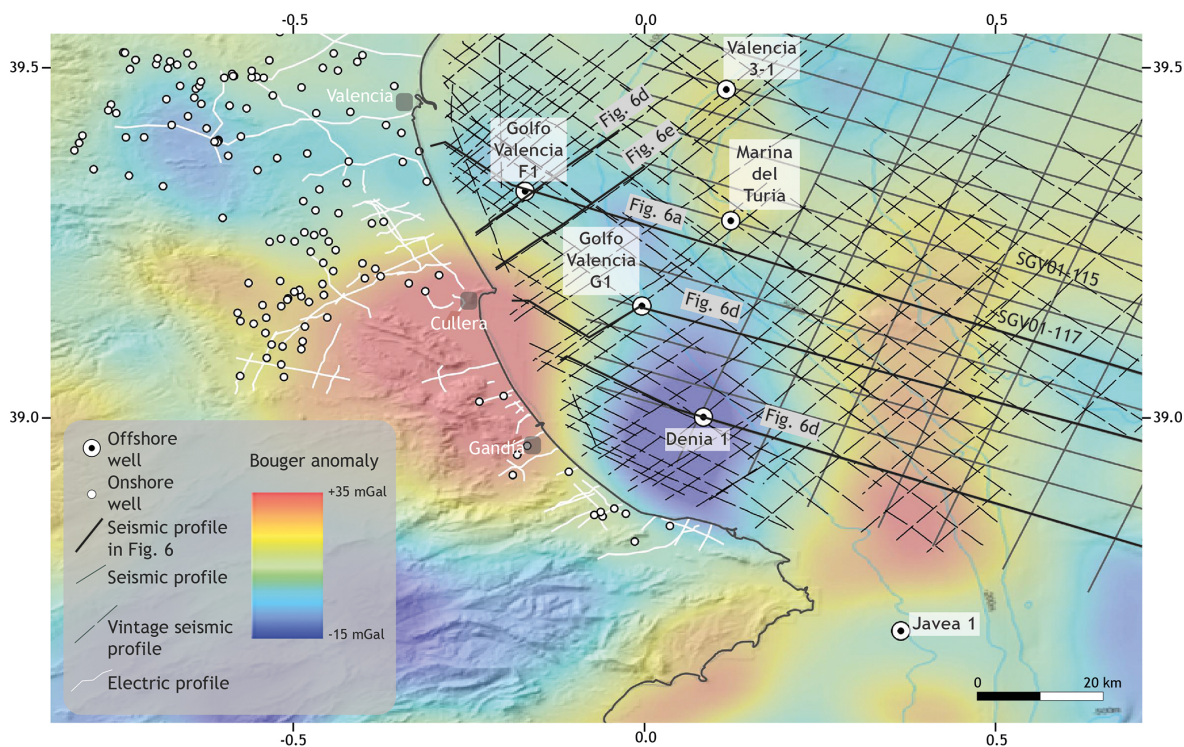


Figure 3. Geophysical dataset used in this work. Filtered Bouguer anomaly data after Getech (2015). The location is shown in Fig. 1.

drilled (Jaraco-1 and Perenchiza-1). However, stratigraphic information is available from 95 hydrogeological wells in the Valencia coastal plain, as are vertical electric sounding (VES) profiles acquired for hydrogeological surveys. The data are publicly available in the online IGME-CSIC databases IRYDA, BD Puntos Agua 2.0 and Sistema de Información Documental (SID) (accessible through <https://info.igme.es/catalogo/>, last access: 15 March 2025).

In areas with poor seismic coverage, structural mapping was aided by regional Bouguer gravity anomalies processed with a Butterworth high-pass filter with a 1° cut-off frequency to highlight short-wavelength features of the data (by Getech, 2015).

4 Stratigraphy

The general stratigraphic arrangement of the southwestern Valencia Trough (Fig. 4) consists of a rigid Palaeozoic–Middle Triassic basement overlain by a 1.5–7 km Upper Triassic–Quaternary stratigraphic cover. Here we present a new detailed stratigraphic framework for the late Miocene–Quaternary of the southern Valencia Trough. The definition of the pre-Neogene stratigraphic units presented in this work is based on mainly previous literature and our analysis of well data, as well as outcrops in the mainland for the most recent sediments.

The Upper Triassic succession (Fig. 4) consists of evaporites, shales and dolomites (Keuper Facies) (Vargas et al., 2009). The Upper Triassic deposits are overlain by Early Jurassic to Late Cretaceous carbonates and marls (Salas et al., 2001), erosive, angular unconformity that is directly overlain by Neogene deposits. The Cenozoic succession starts with a transition from continental clastic sediments to marine platform carbonates, ending with a deposit formed by progradational terrigenous shelf-talus sediments (Arche et al., 2010; Clavell and Berástegui, 1991; Etheve et al., 2018; Lanaja, 1987; Maillard et al., 1992; Ribó et al., 2016b, a; Roca and Desegaulx, 1992; Soler y José et al., 1983). The Neogene succession onshore of the southwestern Valencia Trough (Fig. 4) mostly consists of middle–late Miocene continental to marginal marine deposits, including limestones, marls and coarse-grained detrital sediments. The top of the Miocene series is an erosional unconformity (Messinian Erosion Surface (MES) (Stampfli and Höcker, 1989; Lofi et al., 2011; Cameselle et al., 2014).

Pliocene–recent sediments form a large prograding shelf complex with prominent clinoforms visible in seismic data, which downlap onto the MES. Prominent undulations on slope foresets are visible on most seismic lines and are interpreted as sediment waves (Ribó et al., 2016a). In the offshore wells, the stratigraphic succession consists of an overall shallowing-upward series of thick grey claystones with calcareous interbeds at the base, grading upwards into sandstones and shell beds at the top. No unconformities have been

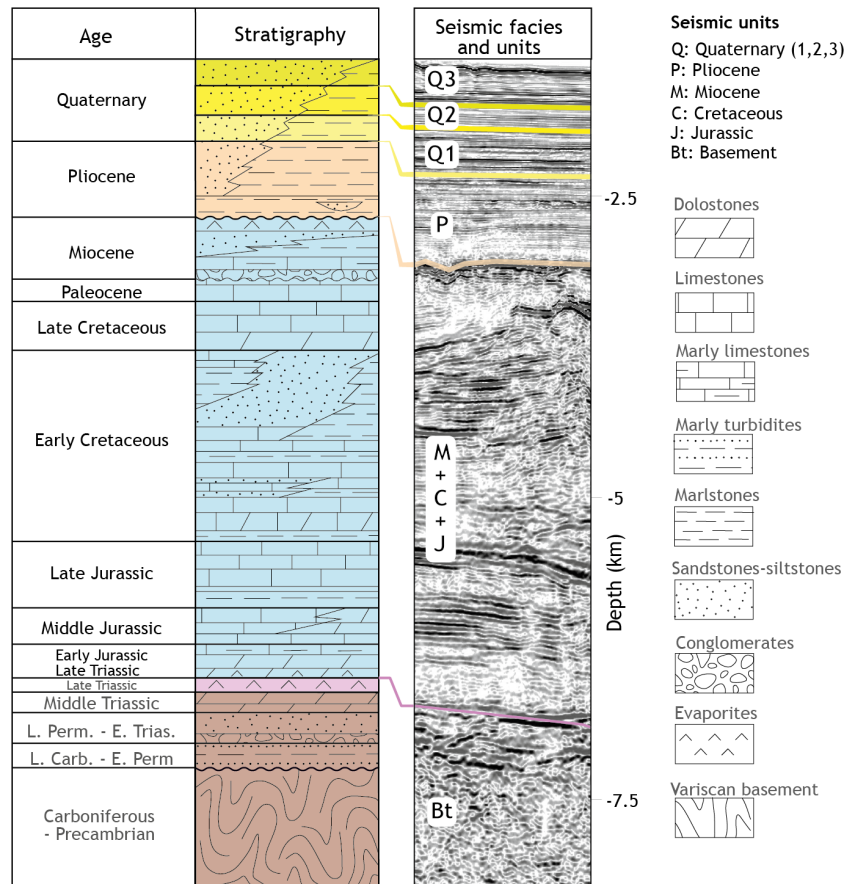


Figure 4. Chronostratigraphic diagram of the southwestern Valencia Trough. Note that the depth scale shows maximum thicknesses of the units. Modified from Ramos et al. (2025).

identified in the entire sequence, except for erosional gullies and canyons at the shelf edge. The Plio-Quaternary sequence reaches a maximum thickness of approximately 3000 m.

To determine the Plio-Quaternary depositional history and slip rate of major faults, six seismic horizons have been mapped and dated with palaeontological data from offshore wells, via the biostratigraphic scheme of Lirer et al. (2019). Starting from the Messinian unconformity at 5.3 Ma, seismic markers have been dated at 3.8 Ma (LO of *G. margaritae*), 3.3 Ma (FO *G. bononiensis*), 2.6 Ma (LCO *G. obliquus*) and 2.0 Ma (FO *G. truncatulinoides*). As no samples were collected from any of the offshore wells above the lower-middle Pleistocene interval, an additional marker (approximately 1.0 Ma) was picked halfway through the 2.0 Ma marker and seabed (0 Ma), assuming a constant sedimentation rate.

Isopach maps (Fig. 5) were produced for the intervals of Pliocene (MES to 2.6 Ma marker) and Pleistocene–recent (2.6 Ma marker to the seabed), revealing a significant shift in the location of the depocentre. The Pliocene depocentre is located very close to the southern coast near Denia, attaining a maximum thickness of approximately 1500 m, whereas the Pleistocene depocentre has prograded ca. 20 km to the

NNW, reaching a thickness of more than 1750 m. The western shoreward edge of both the Pliocene and Pleistocene depocentres is controlled by very large NNW–SSE-trending normal faults (see below).

The described stratigraphic architecture indicates significant mechanical layering in the southwestern Valencia Trough. A rigid basement is overlain by a mechanically weak layer represented by the Upper Triassic Keuper Facies. Above this interval, a rigid Mesozoic carbonate succession is present, followed by a semirigid layer composed of primarily detrital deposits.

5 Main active faults in the southwestern Valencia Trough

In this section, we describe the main structural features of the southwestern Valencia Trough after the analysis of gravity data and isopach maps obtained from the subsurface dataset (seismic lines, wells and VES) (Figs. 3 and 5).

The filtered Bouguer anomaly map (Fig. 3) reveals a positive anomaly in the central part of the study area, referred to as the Cullera anomaly. This positive anomaly is surrounded

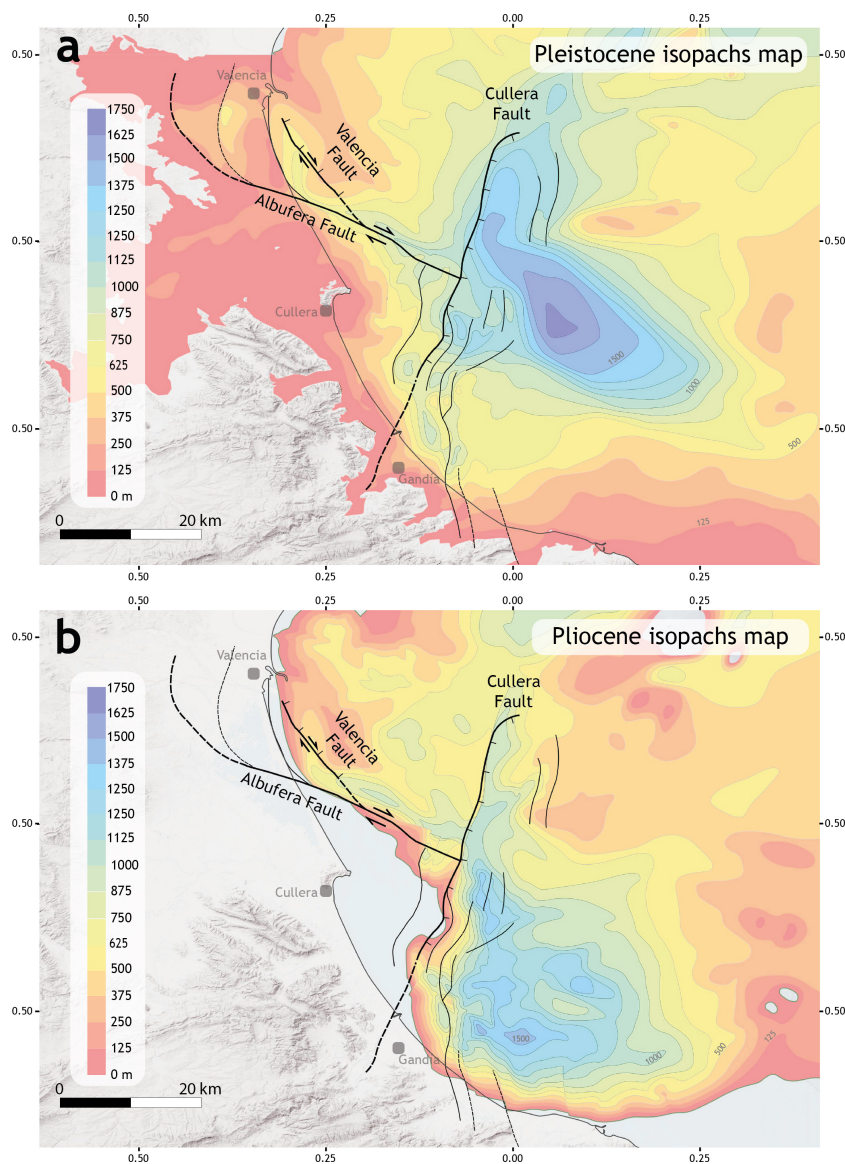


Figure 5. Isopach maps of the southwestern Valencia Trough for the Pleistocene (a) and Pliocene (b). The traces of the active faults are also depicted. Fault traces represent the horizontal projection of the direction line of the fault plane, located midway between the intersection line of the top-of-the-Pliocene horizon and the top-of-the-Quaternary horizon. Fault traces are derived primarily from their position on seismic profiles, supplemented by isopach maps and observed thickness variations in stratigraphic units, as indicated by the available wells. Dashed lines show interpreted traces. Modified from Ramos et al. (2025).

by a region exhibiting a negative anomaly, particularly in the offshore area located east of Cullera. We interpret this pattern of anomalies to be because of mass excess associated with a basement high (Cullera positive anomaly) surrounded by a region with greater sedimentary cover (negative anomaly). This interpretation is further supported by the isopach maps derived from interpretation of the subsurface data (Fig. 5). The negative gravity anomaly correlates with an abrupt increase in the thickness of both the Pliocene and Quaternary sedimentary successions. Furthermore, the transitions in both the gravity anomaly and sedimentary thickness correspond

to the positions of the main faults observed in the seismic dataset (see below). On the basis of this evidence, we propose that the southwestern Valencia Trough is structurally characterised by the presence of three major faults offsetting the basement and significantly influencing the stratigraphic evolution of the area. These three major faults are: the Cullera Fault, the Valencia Fault and the Albufera Fault (Fig. 5).

The structural configuration of the southwestern Valencia Trough is also influenced by the presence of Upper Triassic evaporites and shales at the base of the Mesozoic sedimentary cover. Major faults offsetting the Mesozoic–Quaternary

succession present a listric geometry with a main ramp that flattens out in the Upper Triassic salt layer (Fig. 6). These geometries have been interpreted as evidence of a strain partitioning between the suprasalt and the subsalt successions (Etheve et al., 2016; Fang et al., 2021; Ramos et al., 2025). According to these interpretations, the Upper Triassic is a mechanically weak layer that induces tectonic decoupling within the seismogenic crust of the southwestern Valencia Trough. As a result, the deformation style of the suprasalt succession (cover) differs significantly from that of the subsalt succession (basement) (Etheve et al., 2018; Fang et al., 2021; Ramos et al., 2023, 2025; Roma et al., 2018). The main difference is that normal faults present a listric geometry in the cover, while these faults are planar within the basement (see below).

The analysis of the seismic reflection profiles (Fig. 6) reveals three fault types: (i) faults restricted to the subsalt basement; (ii) faults restricted to the suprasalt cover; and (iii) faults cutting through the sedimentary cover, basement and salt layer.

5.1 Cullera Fault

The Cullera Fault is the longest along-strike fault in the region, spans approximately 59 km, and has the highest cumulative offset, with more than 1800 m of vertical displacement at the top of the Messinian horizon (Figs. 5 and 6).

The along-section geometry of the fault across the suprasalt succession is well imaged in the seismic reflection dataset (Fig. 6). The Cullera Fault is a normal, NNE–SSW-trending fault that dips highly towards the east. The fault offsets the entire suprasalt cover, including the 1 Ma horizon. Owing to the low resolution of the available bathymetric data, it is not possible to confirm whether the fault offsets the seafloor. The Cullera Fault displaces the top of the basement horizon, indicating that this fault involves both subsalt and suprasalt successions.

Within the basement, the Cullera Fault is poorly imaged in seismic profiles. Nevertheless, the available data suggest that it is a planar fault (Fig. 6). This is also supported by the absence of significant tilting of the basement-top horizon.

In contrast, the geometry of the Cullera Fault in the sedimentary cover is heterogeneous. In the northern area (Fig. 6), the part of the Cullera Fault offsetting the cover exhibits a listric geometry, which is responsible for the development of a rollover structure in the hanging wall (Fig. 6). Southwards, the listric geometry and related rollover fold becomes less pronounced (Fig. 6).

To better constrain the geometry of the Cullera Fault, we constructed a structural map of the fault by integrating fault traces identified in the seismic reflection dataset with isopach maps (Fig. 7). Additionally, a 3D model of the Cullera Fault, along with the two other major faults, was generated following a 2.5D construction approach, integrating interpreted seismic profiles via interpolation. We employed the ordi-

nary kriging algorithm implemented in MOVE software, a methodology consistent with previous approaches applied to analogous structures (Ramos et al., 2020). Analysis of the reconstructed 3D fault indicates that the surface area of the Cullera Fault offsetting the sedimentary cover is approximately 360 km².

Several minor normal faults have developed in the hanging wall of the Cullera Fault (Fig. 5). These faults displace only the suprasalt succession without affecting the underlying subsalt units. In previous studies (e.g., Perea, 2006; Roca, 1992), distinct names were assigned to these faults, such as the Western Cabo Cullera Fault, Central Cabo Cullera Fault, and Eastern Cabo Cullera Fault. However, the improved resolution and quality of the new seismic dataset enable a more detailed characterisation of these tectonic structures, allowing for a reassessment of their nomenclature and role. We interpret these minor faults to be part of the damage zone associated with the main Cullera Fault.

The quality of the seismic dataset allows for an analysis of the slip rate of the Cullera Fault. This analysis is approximate, because of the resolution of the seismic profiles, the uncertainties in the recognition of the markers in the hanging wall and footwall, and the age of these markers. Net slip rates were obtained for the Top-Messinian, Top Pliocene, Top-Q1, and Top-Q2 horizons, with assigned ages of 5.3, 2.6, 2, and 1 Ma, respectively (Fig. 8). The slip rates for the Cullera Fault seem to have decreased over time, as the calculation yielded mean slip rates of 0.40 ± 0.1 mm yr⁻¹ for the Pliocene and 0.15 ± 0.1 mm yr⁻¹ for the Quaternary. This slip rate reduction could be the consequence of a change in the regional tectonic regime in the complex tectonic cadre of the western Mediterranean region. However, as the Cullera Fault is a salt-influenced structure, different mechanisms control fault offset. We discuss in Sect. 6 the potential reasons behind this observed decrease in slip rate. In any case, we cannot dismiss that at least part of this apparent in-time evolution could be an artefact related to the epistemic uncertainties mentioned above.

5.2 Albufera Fault

The Albufera Fault (Figs. 5 and 6) is a newly defined active structure in the southwestern Valencia Trough. This NW–SE striking fault extends approximately 55 km and presents an oblique kinematic, with a major strike slip component and a minor normal displacement (see below). The Albufera Fault exhibits a maximum vertical offset of 1000 m for the Top-Messinian horizon. This would imply a long-term vertical slip rate of 0.2 ± 0.1 mm yr⁻¹. The fault offsets both the supra- and subsalt successions (Figs. 5 and 6). The Albufera Fault is visible only in the vintage seismic reflection dataset, where it presents a low dip and a listric geometry.

The Albufera Fault appears to offset the entire suprasalt cover, including the 1 Ma horizon. As with other faults in the region, the low resolution of the available bathymetric

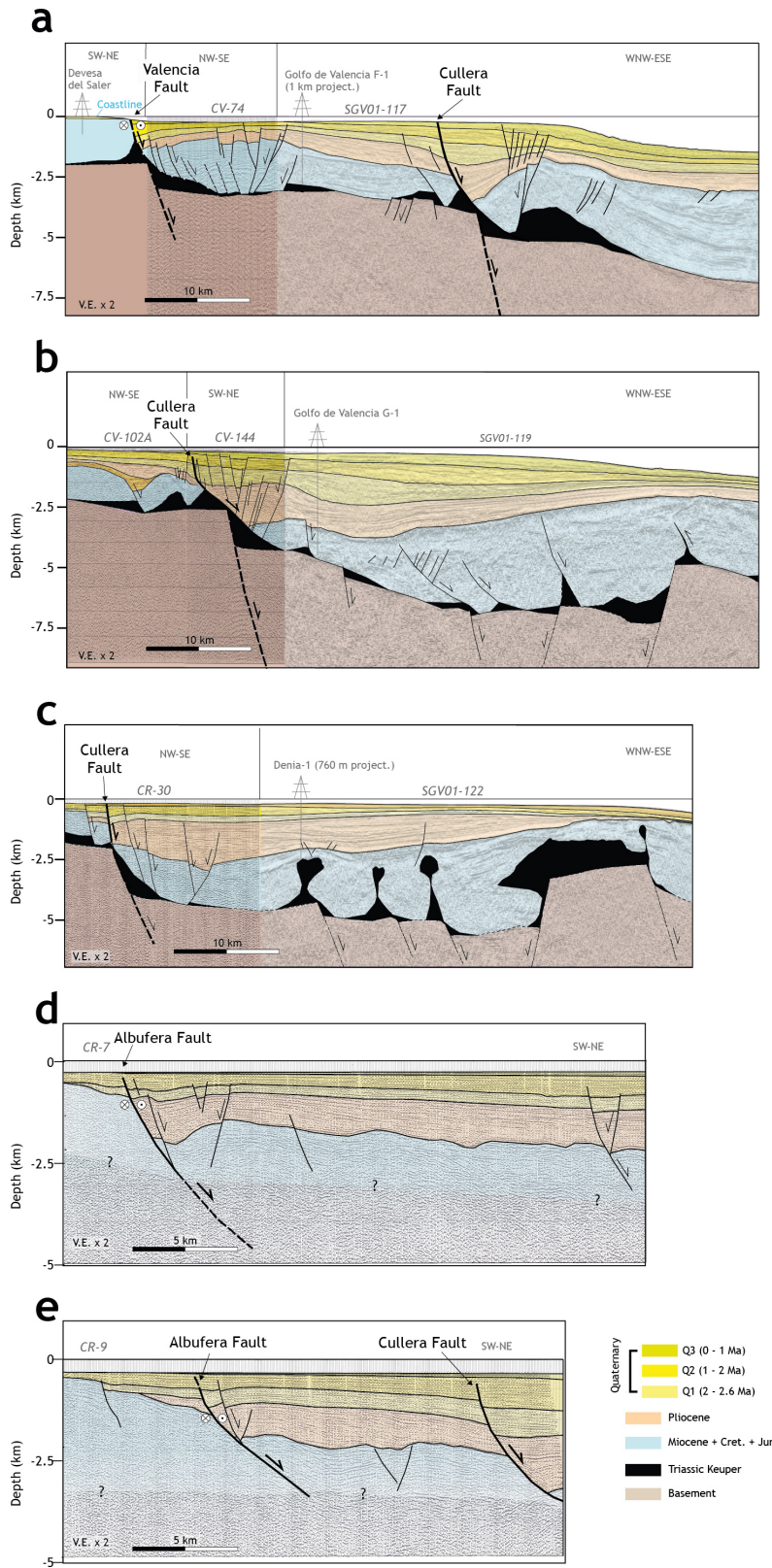


Figure 6. Interpreted sections derived from onshore cross-sections (a) and the offshore 2D seismic profiles (a–e). Sections in panels (a)–(d) depict the structure of both the supra- and subsalt successions, while in sections in panels (d)–(e) only the suprasalt structure is represented. See Fig. 3 for the location. (a–c) Sections after Ramos et al. (2025). Unit colours are as those in Fig. 4 (except for the Triassic unit). Note the $\times 2$ vertical exaggeration of all the sections.

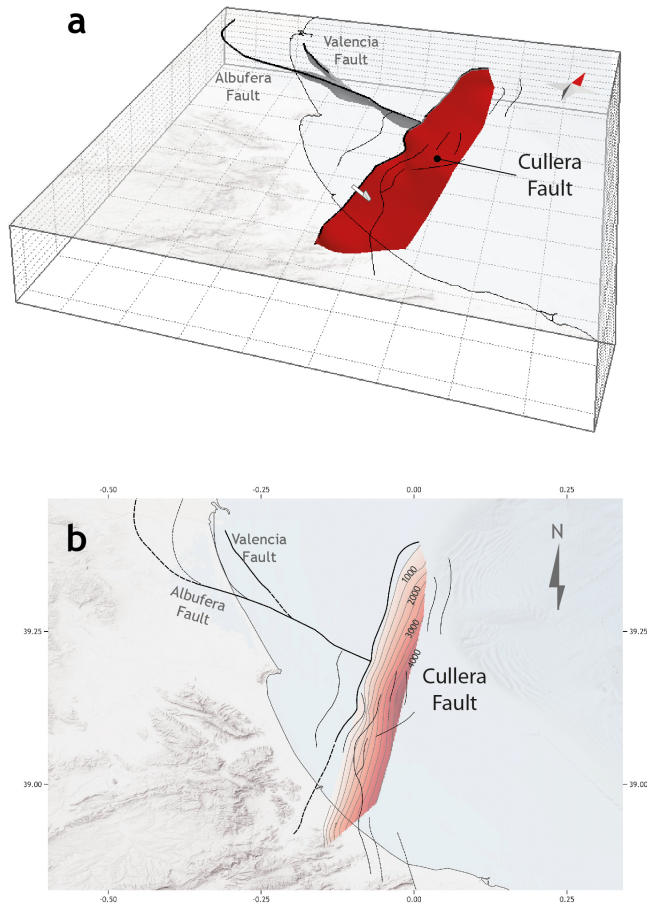


Figure 7. 3D model (a) and structural map (b) of the Cullera Fault (red surface). Squares in panel (a) represent 10 km × 10 km. Note the red arrow pointing to the north in panel (a).

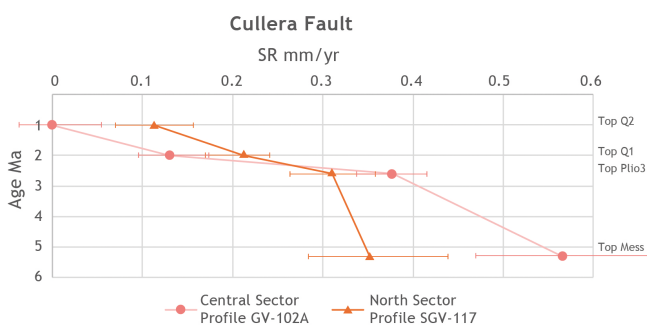


Figure 8. Long term slip rates (SR) for the Cullera Fault derived from the seismic profiles for the Top Messinian, Top Plio3, Top Q1, and Top Q2 horizons. The pink line and dots represent SR for the central sector of the fault. The orange line and triangles indicate SR for the north sector of the fault. The slip rates seem to decrease in time, from $0.40 \pm 0.1 \text{ mm yr}^{-1}$ for the Pliocene to $0.15 \pm 0.1 \text{ mm yr}^{-1}$ for the Quaternary. Error bars are estimated on the basis of uncertainties in the recognition of the markers and their ages.

data prevents us from determining whether this fault offsets the seabed. Nevertheless, high-resolution seismic profiles from the offshore shelf analysed by previous authors indicate seabed offsets caused by secondary normal faults likely associated with the Albufera Fault (Díaz de Rfo et al., 1986; Albarracín et al., 2013).

The available seismic dataset reveals a normal kinematic component for the Albufera Fault. However, mapping of small-scale fault traces in upper Pleistocene–recent sediments (interval between the seabed and the 1.8 Ma horizon) reveals that these faults are oblique to the main trend of the Albufera Fault, forming an en echelon pattern in map view, which suggests that the Plio-Quaternary reactivation of the main fault has a significant right-lateral strike-slip component. This dextral component is consistent with the regional ENE–WSW direction of Plio-Quaternary extension in the southwestern Valencia Trough and kinematically consistent with NNW–SSE trending normal faults. The fault influences the Plio-Quaternary sedimentary infill of the southwestern Valencia Trough (Fig. 5). The isopach maps reveal that the Pliocene and Quaternary succession significantly increased in the hanging wall relative to the footwall. The listric geometry of the Albufera Fault is responsible for the development of a rollover anticline in the hanging wall (Fig. 6). This anticline is likely accentuated by the palaeoshelf edge of the late Tortonian–early Messinian shelf, which is located in the central part of the rollover structure.

To further constrain the geometry of the Albufera Fault, a structural map and a 3D model of the fault was constructed (Fig. 9). Analysis of the reconstructed 3D fault surface indicates that the fault encompasses an area of approximately 560 km^2 .

5.3 Valencia Fault

In this section, we describe the Valencia Fault (Figs. 5 and 6). This structure could correspond to the Western Cabo Cullera Fault (*sensu* Perea, 2006). The Valencia Fault presents a length of approximately 20 km and has a significant impact on the distribution of Quaternary depocentres. The Valencia Fault presents a normal component, as it vertically displaces both the supra- and subsalt successions (see below) (Figs. 5 and 6). However, taking into account the general structural arrangement of the southwestern Valencia Trough, we postulate that the Valencia Fault presents also a strike-slip component.

This NNW–SSE trending, steeply dipping fault is imaged primarily in the vintage seismic reflection dataset, where it exhibits a listric geometry, at least in the portion offsetting the suprasalt succession (Fig. 6). The Valencia Fault vertically offsets the entire suprasalt cover, including the 1 Ma horizon. However, owing to the low resolution of the available bathymetric data, it is not possible to determine whether this fault offsets the seabed. The Valencia Fault also displaces vertically the top of the basement horizon, indicating

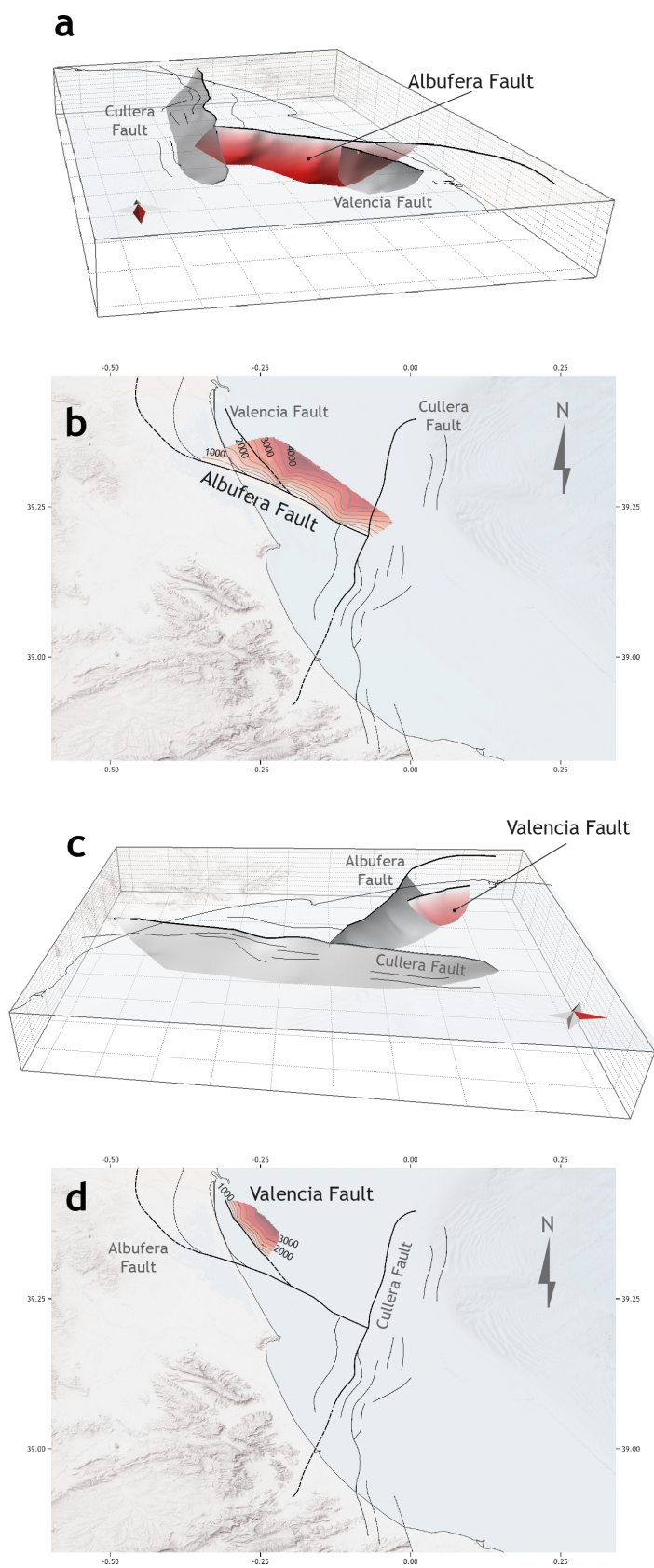


Figure 9. 3D model and structural map of the Albufera Fault (a, b) and the Valencia Fault (c, d). Squares in the 3D models represent 10 km × 10 km boxes. Note the red arrow pointing to the north in panels (a) and (c).

that this structure involves both subsalt and suprasalt successions. Within the basement, the Valencia Fault is not well-imaged in the seismic profiles, but the absence of tilting in the basement-top horizon suggests that it is a planar fault (Fig. 6). The Valencia Fault and its secondary strands very likely continue onshore below the City of Valencia. The lack of onshore seismic data hampers the mapping of these fault strands, but their presence can be inferred from the abrupt Plio-Quaternary thickness changes observed in water wells and vertical electric sounding profiles.

To further constrain the geometry of the Valencia Fault, a structural map and a 3D model of the fault was constructed (Fig. 9). Analysis of the reconstructed 3D fault surface indicates that the fault encompasses an area of approximately 208 km².

6 Evolutionary growth of the Cullera Fault: interplay between tectonics and salt withdrawal

This section aims to provide further insights into the evolution of the active faults in the southwestern Valencia Trough. The low resolution of the vintage seismic dataset limits the ability to perform a detailed analysis only for the Cullera Fault. To analyse recent along-dip variations in throw, we constructed throw-depth plots (T - z plots) for the post-Messinian markers (Fig. 10). These plots provide insights into the evolutionary growth of the fault (Mansfield and Cartwright, 1996; Hongxing and Anderson, 2007). The quality of the available seismic reflection dataset allows this analysis to be performed on two seismic profiles located in the northern part of the fault, where the listric geometry is well-developed (LINES SGV01-115 and SGV01-117; Figs. 3 and 6).

We computed T - z plots for six suprasalt horizons: Top-Messinian, Top Plio1, Top Plio2, Top Plio3, Top Q1, and Top Q2 (Fig. 10). The T - z plots for the Cullera Fault reveal a general increase in the throw and throw gradient with depth. We postulate that the increase observed in the throw is the result of the differing ages of the horizons, older horizons show greater offset because they have been displaced over a longer time interval. As regards throw gradients, the data indicate two distinct portions: (i) the lower portion, with higher throw gradients, includes horizons from the Top Messinian to the Top Pliocene; (ii) the upper portion, with lower throw gradients, comprises the Quaternary horizons. This distinction is particularly pronounced in the southern seismic line (line SGV01-117, Fig. 6). Here, the throw gradient decreases, from 2.38–2.98 in the lower portion to 0.22–0.10 in the upper portion.

The Cullera Fault significantly influences the Plio-Quaternary sedimentary infill of the southwestern Valencia Trough. Isopach maps indicate a marked increase in the thickness of both Pliocene and Quaternary successions in the hanging wall with respect to the footwall (Fig. 5). To

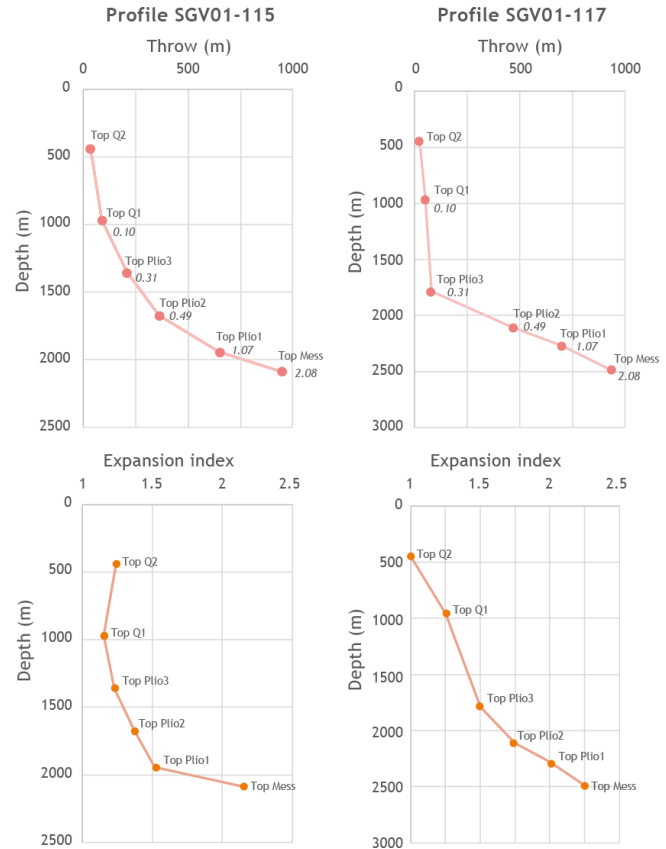


Figure 10. Throw depth (T - z) and expansion index plots for the Cullera Fault computed from profiles SGV01-115 and SGV01-117. The numbers within the T - z plots indicate the throw gradient for the corresponding interval. The T - z plots reveal an increase in the throw and throw gradient, with a higher throw gradient for the Top Messinian–Top Pliocene interval and a lower throw gradient for the Quaternary interval.

quantify this relationship, we computed the expansion index (Thorsen, 1963; Rouby et al., 2003; Jackson and Rotevatn, 2013) for the post-Messinian stratigraphic units (Fig. 10). The expansion index consistently exceeds 1 across all the analysed intervals, indicating a synkinematic deposition in these units. The Pliocene units exhibit a greater expansion index than the Quaternary units do, with the difference being particularly pronounced in the southern seismic line (Fig. 6 LINE SGV01-117).

Finally, to shed light on the mechanisms controlling the creation of accommodation space related to the Cullera Fault, we analyse the tectonic–stratigraphic arrangement of the hanging wall units. To discuss this point, we compare the geometries observed in the southwestern Valencia Trough with analogous stratigraphic geometries in the Danish North Sea, where they have been interpreted in terms of the evolution of salt-influenced faults (Duffy et al., 2023 and references therein). In such a setting, two mechanisms create accommodation space: fault displacement and load-driven salt with-

drawal in the hanging-wall. These two mechanisms can act separately or contemporaneously in time. When the accommodation space generated by the fault offset exceeds that created by salt withdrawal, the depocentre axis remains adjacent to the fault. In contrast, when salt-related accommodation space is dominant, the depocentre migrates away from the fault (Duffy et al., 2023).

In the northern part of the Cullera Fault, where the rollover structure is well developed (Fig. 6), the position of the Plio-Quaternary depocentre in the hanging-wall varies along the dip direction. The Pliocene depocentre remains in the immediate hanging wall of the fault. Therefore, we interpret that, during the Pliocene, the accommodation space generated by the displacement of the Cullera Fault exceeded that produced by the accommodation space related to salt withdrawal. During the deposition of unit Q1, the depocentre migrated basinwards, suggesting that salt withdrawal-related accommodation space outpaced that related to fault displacement. Finally, during Q2 and Q3, the depocentre axis shifted towards the fault, indicating that fault displacement-related accommodation space regained dominance over salt mobility. We postulate that this evolution in the location of depocentres is related to the mechanisms responsible for the creation of accommodation space.

All the above-described features shed light on the evolution of the salt-influenced Cullera Fault. As previously discussed, the creation of accommodation space results from two mechanisms: tectonic offset along the fault and displacement related to salt withdrawal. Both mechanisms act cumulatively; that is, both mechanisms produce slip along the Cullera Fault and create accommodation space. The migration of successive depocentres suggests that, during the Pliocene, accommodation space related to tectonic offset was greater than that created by salt withdrawal. As the throw gradient is high (≈ 2.4) during this period, we postulate that both mechanisms were active. During the deposition of Q1 (2.6–2 Ma), the position of the depocentre suggests that salt mobility became the dominant mechanism, likely due to a decrease in fault activity, an increase in salt withdrawal, or both. As throw gradient decreases during this period, we postulate that a decrease in the fault displacement rate could be the reason for the change in the main mechanism. Finally, during the rest of the Quaternary (2 Ma to present), fault displacement-related accommodation space once again exceeded that created by salt withdrawal. The constant throw gradient observed during this period with respect to the previous time interval (2.6–2 Ma) suggests that the change in the main mechanism was due to a reduction in or cessation of salt withdrawal. This interpretation is further supported by the off-fault geometry of the Q2–Q3 sedimentary bodies, as no significant change in thickness is observed above the salt withdrawal-related anticlinal crest located east of the Cullera Fault (Fig. 6).

Therefore, according to the above exposed, we postulate that, during the Pliocene and lower Quaternary (up to 2 Ma

ago), the offset of the Cullera Fault was produced by both tectonics and salt withdrawal, being the first mechanism dominant during the Pliocene and the second during the 2.6–2 Ma time span. From that moment to the present salt withdrawal ceases (or significantly reduces), and tectonics becomes the only (or very dominant) process. The reduction of salt movement is possibly due to the complete withdrawal of mobile salt and the formation of a weld below the hanging wall. This evolution could also explain the slip rate decreases observed for the Cullera Fault (Fig. 8). A higher slip rate is expected during the Pliocene, when both tectonics and salt withdrawal were active. Once salt withdrawal ceases or significantly decreases, a corresponding decrease in the slip rate is also expected.

7 Influence of mechanical layering on the seismic potential: the case of the southwestern Valencia Trough

The southwestern Valencia Trough has a distinct mechanical stratigraphy characterised by three layers: a subsalt basement, a weak mechanical layer composed of Triassic evaporites, and overlain Mesozoic–Quaternary sedimentary succession. Triassic evaporites are well documented for their ductile behaviour, which enables them to act as regional detachment layers (e.g., Morley et al., 2003; Jackson and Hudec, 2005) and inhibits the propagation of faults (e.g., Withjack et al., 1990; Pascoe et al., 1999; Maurin and Niviere, 1999; Withjack and Callaway, 2000; Richardson et al., 2005; Ford et al., 2007; Kane et al., 2010; Marsh et al., 2010). Moreover, mechanically weak layers have been shown to induce full or partial geometric and kinematic decoupling between sub- and supradetachment successions (e.g., Stewart et al., 1997; Withjack and Callaway, 2000; Ford et al., 2007; Tvedt et al., 2013). In this section, we focus on the implications of this mechanical arrangement in terms of how the presence of a weak mechanical layer influence the vertical propagation of seismic ruptures.

In an active region, tectonics are generally the main driving mechanism of fault displacement. However, in the case of salt-influenced faults, displacement can also result from salt withdrawal. Our analysis of the evolution of the Cullera Fault presented in the previous section indicates that the fault offset is related to the interplay between two mechanisms: tectonic offset along the fault and displacement related to salt withdrawal. Our analysis also reveals how these two processes interact with each other. Consequently, in areas with salt-influenced faults, seismicity can potentially be produced from either mechanism or a combination of both.

In terms of seismic potential, there is a significant difference between a tectonic earthquake and a salt-withdrawal earthquake. This difference lies in the maximum potential thickness of the seismogenic layer involved in the rupture. Tectonic stress affects the entire crust; therefore, strain re-

lated to tectonic accumulates both in the suprasalt and subsalt successions. Consequently, a tectonically driven earthquake could theoretically rupture the entire seismogenic crust. In contrast, a salt withdrawal-related earthquake would imply offset restricted to the suprasalt succession, as in this case displacement surface coalesces into the salt layer. Therefore, in an earthquake restricted to the suprasalt succession, the thickness of the seismogenic layer is limited by the depth of the mechanically weak layer, reducing the maximum potential rupture area and, consequently, the seismic potential. A salt-withdrawal-related earthquake could induce a vertical stress drop related to salt displacement, potentially triggering displacement in the subsalt succession and leading to a complex rupture. Similarly, a tectonically driven earthquake may rupture only the suprasalt succession.

Despite the mechanism driving seismicity, the presence of a weak mechanical layer within the seismogenic crust significantly influences the seismogenic potential of active faults. We hypothesise that this weak layer could locally hinder the effective vertical propagation of a rupture, thereby resulting in faults being seismogenically bounded. Specifically, the total or partial decoupling induced by the weak evaporitic layer may limit the effective width of the seismogenic layer. This hypothesis is independent of the weak layer composition; therefore, our hypothesis can be extended to any region with a similar structural configuration.

Significant earthquakes ($M_w > 6$) typically nucleate at depths greater than 5 km. However, recent events in central Italy and France have demonstrated that very shallow (2–5 km) earthquakes of moderate magnitude (M_w 5–6) can also occur (Chiaraluce et al., 2017; Godano et al., 2025; Improta et al., 2019). In the southwestern Valencia Trough, the thickness of the supra-salt succession is slightly less than 5 km. Therefore, while the probability of a significant earthquake nucleating within the supra-salt succession is low, it is not zero. In this section we evaluate the seismic potential of these (unlikely) supra-salt ruptures. The case of central Italy could be taken as a geologic and tectonic analogous of the southwestern Valencia Trough. Central Italy resembles the southwestern Valencia Trough as both regions are presently dominated by extensional tectonics, and both are characterised by a pronounced mechanical layering in the upper crust. Recently, central Italy has undergone high seismicity, including the 1997–1998 Umbria-Marche, 2009 L'Aquila, and 2016–2017 Amatrice-Norcia seismic sequences (Chiaraluce et al., 2003; Valoroso et al., 2013; Chiaraluce et al., 2017; Improta et al., 2019; Michele et al., 2020). The area of central Italy where these seismic sequences took place is characterized by a complex geological framework consisting of several geological domains. Most of this area belongs to the Umbria-Marche fold-and-thrust belt. This belt consists of a crystalline basement overlain by a 3–8 km-thick Mesozoic–Quaternary sedimentary cover (Cresta et al., 1989; Centamore et al., 1992; Menichetti and Coccioni, 2013). The sedimentary Mesozoic succession starts with a 1.2 km thick

salt layer (Anidriti di Burano Formation; Martinis and Pieri, 1964) acting as a mechanical weak layer. That is, similar to the southwestern Valencia Trough, the seismogenic crust of central Italy is characterised by the presence of a mechanically weak layer. As a consequence of thrusting during the Miocene-Pliocene, this weak layer is vertically repeated in some sectors (Barchi et al., 2021). Therefore, in central Italy the seismogenic crust includes from one to three weak layers.

Central Italy undergoes extension responsible for normal active faults. These active normal faults are the seismogenic sources of the seismic sequences occurred in the last decades (e.g., Boncio et al., 2004; Barchi and Mirabella, 2009), as well as several historical events (Rovida et al., 2020). Normal active faults in central Italy present a listric geometry in the sedimentary cover and offset the top of the basement (Barchi et al., 2021). The 1997–1998 Umbria-Marche and 2016–2017 Amatrice-Norcia seismic sequences nucleated within the suprasalt succession, including main events (M_w 5–6) with very shallow centroids (3–4 km; Barchi et al., 2021).

Based on the tectonic and stratigraphic similarities above exposed, we propose that the southwestern Valencia Trough may exhibit a comparable pattern of seismicity to that of central Italy. Specifically, we hypothesise that seismic events in the southwestern Valencia Trough could also have nucleated within the suprasalt succession and in the basement. Furthermore, we postulate that large earthquakes in the southwestern Valencia Trough could also rupture both mechanical layers. Available centroid data for the southwestern Valencia Trough suggest that most earthquakes nucleate at depths between 1 and 13 km (Fig. 2). Although these depth estimates carry significant uncertainties, we interpret this dataset as supporting evidence for our hypothesis that seismicity in the southwestern Valencia Trough nucleates both in the basement and in the cover.

From this hypothesis we evaluate the seismic potential of these (unlikely) supra-salt ruptures. A widely used approach to characterise the seismic potential of an active fault involves earthquake fault scaling relationships. These relationships estimate the seismic parameters of an active fault based on its geometric and/or kinematic features (Kanamori and Anderson, 1975; Geller, 1976; Wells and Coppersmith, 1994; Stirling et al., 2002, 2013; Leonard, 2010, 2014; among many others). In the case of the southwestern Valencia Trough faults, the available data support characterisation on the basis of geometric features, such as fault area, length, or width. However, the mechanical layering observed in the southwestern Valencia Trough necessitates the cautious application of these scaling relationships. The influence of the weak mechanical layer introduces complexities that may not be fully accounted for by traditional scaling methods.

As we mentioned previously, most empirical source-scaling relationships for crustal earthquakes correlate the moment magnitude (M_w) with the fault dimensions (length, width, and/or area; Kanamori and Anderson, 1975; Geller,

1976; Wells and Coppersmith, 1994; Stirling et al., 2002; Leonard, 2010; among many others). We propose that when these scaling relationships are applied to regions with a weak mechanical layer, the role of this layer should be explicitly considered in the analysis. This is because the presence of a weak layer can potentially hinder the effective vertical propagation of a rupture, thereby limiting the effective width of the seismogenic layer. This consideration is particularly relevant for earthquakes that nucleate above the weak layer. We propose including a correction factor in the empirical relationships that explicitly accounts for cases where earthquakes are more likely to involve only part of the seismogenic layer due to mechanical heterogeneities within the crust. This factor would aim to provide a more accurate seismic characterization of faults in regions with such a structural arrangement.

Several studies suggest that the downdip width of the seismogenic crust (the thickness of seismogenic crust measured along the fault plane) can constrain the maximum magnitudes of earthquakes (Hyndman et al., 1997; Ruff and Kanamori, 1983; Weng and Yang, 2017). For large-magnitude events involving the entire seismogenic crust, some scaling relationships account for the constraint on fault-width rupture growth relative to fault-length rupture growth by incorporating a change in slope in width-to-length scaling (Leonard, 2010; Yen and Ma, 2011; Leonard, 2014; Cheng et al., 2019; Huang et al., 2024). This change in slope reflects the width of the seismogenic crust, which imposes a limit on rupture propagation owing to variations in the mechanical behaviour of the crust. We propose a similar approach to evaluate the seismic potential of regions characterised by a weak mechanical layer within the upper crust, such as the southwestern Valencia Trough.

Our approach involves including the rupture aspect ratio when calculating the geometric parameters of an active fault. Specifically, we propose that, instead of using the total area or length of the fault as direct inputs to scaling relationships, a correction factor should be applied to these geometric parameters. This correction factor is based on the empirical aspect ratio of faults. For example, consider an earthquake nucleating above a weak mechanical layer. Two potential scenarios for the propagation of such an earthquake can be envisioned: (i) that it propagates through the basement–cover interface or (ii) that it remains restricted to the succession above the weak layer. In the first scenario, the potential maximum rupture area can be calculated by multiplying the fault length by the fault width. Any area-based or length-based scaling relationship can then be applied. This scenario represents the maximum seismic potential of the fault.

In the second scenario, where rupture propagation is restricted to succession above the weak layer, a simplistic calculation of the fault area would multiply the total fault length by the thickness of the ruptured succession (Fig. 11). However, since the hypothesised rupture offsets only the succession above the mechanically weak layer, the width of the rupture is significantly limited. This would result in a highly

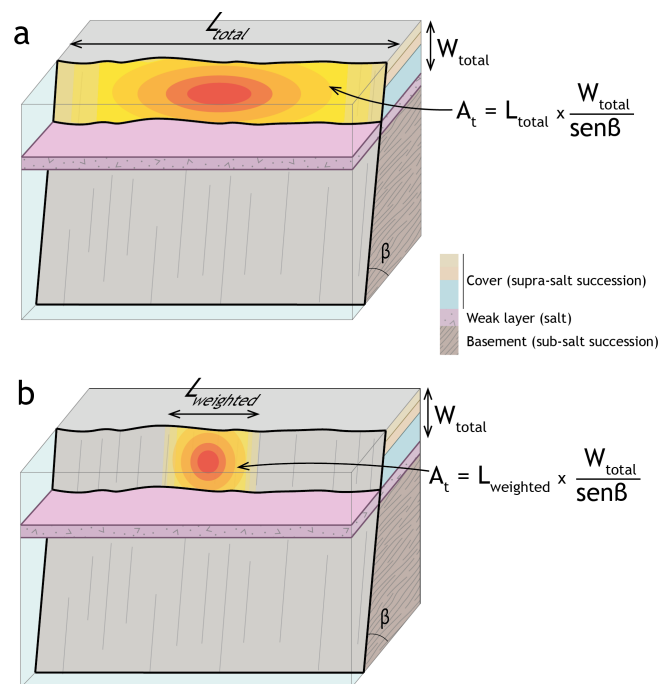


Figure 11. Conceptual model of the weighted rupture area of an earthquake nucleating above the weak mechanical layer. The area of the rupture is shown using a red–yellow gradient. An earthquake rupturing the total fault length (L) and the total thickness (W_{total}) above the weak layer would result in nonrealistic, highly elongated ruptures. In panel (b), we propose a more realistic case: an earthquake offsetting the total thickness above the weak layer (W_{total}) and a rupture length weighted by the aspect ratio (L_w).

elongated rupture with an unusually high aspect ratio, deviating from commonly observed values (Nicol et al., 1996; Stock and Smith, 2000). For this second scenario, we propose using the thickness of the ruptured succession as a limiting factor. Specifically, the rupture area should be calculated by multiplying the width of the fault (based on the thickness of the succession above the weak layer and corrected by the fault dip) by the total fault length weighted by the aspect ratio (Fig. 11). This weighted area can then be used as input in any area-based scaling relationship. We consider that this calculation offers a more realistic estimation of the maximum seismogenic potential for events rupturing only the succession above the weak layer. Finally, we recommend avoiding length-based scaling relations for this second scenario, as such relations implicitly assume a rupture of the entire seismogenic crust.

8 Seismic characterisation of active faults in the southwestern Valencia Trough

In this section, we compute the seismic potential of the active faults in the southwestern Valencia Trough by applying several scaling relationships. We perform two distinct calculations corresponding to the two scenarios described earlier. (i) In the first scenario, we assume a rupture involving both the supra- and subsalt successions. That is, this first scenario accounts for an earthquake rupturing the entire seismogenic crust. This scenario provides the maximum seismic potential of the faults. (ii) In the second scenario, we assume that a rupture is restricted to the suprasalt succession. For this calculation, we apply several area-based scaling relationships, and we use the area weighted by the aspect ratio as the input parameter. Since the rupture area involved in this second scenario is relatively small, a relatively low seismogenic potential is expected.

8.1 First scenario: Ruptures involving the entire seismogenic crust

For both scenarios, we apply the scaling relationships of Wells and Coppersmith (1994) (values corresponding to normal faults for the Cullera and Valencia faults, and to strike slip faults for the Albufera Fault) and Stirling et al. (2002). In the first scenario, i.e., ruptures involving the entire seismogenic crust, we assume that a complete fault ruptured from the subsalt basement through the suprasalt succession. To compute the seismogenic potential of this first scenario we used the fault length and fault area as the primary input parameter (Table 1). The fault area used for these calculations was the result of multiplying the fault length by the fault width. We prefer to use this simplification instead of the areas calculated from our 3D models to ensure consistency when comparing magnitude estimates derived from the methodology involving a correction factor (see below). The total thickness of the seismogenic crust in the study area is not precisely known. García-Mayordomo (2012) proposed a thickness ranging between 9 and 11 km. This value agrees with crust thicknesses based on deep seismic profiles (Etheve et al., 2016; Maillard and Mauffret, 2013; Ramos et al., 2025) as well as the lithospheric structure based on P-wave receiver function analysis and seismic tomography (Mancilla et al., 2015; Palomeras et al., 2017). Therefore, we assumed a mean thickness of the seismogenic crust of 10 km.

8.2 Second scenario: Ruptures involving only the suprasalt succession

In this scenario, the presence of a mechanically weak layer within the seismogenic crust is considered to control the seismic potential of active faults. As discussed previously, we use the weighted rupture area as the input parameter for the scaling relationships. The weighting factor is based on the

aspect ratio of normal faults. To provide context for this approach, we also present seismic parameters calculated from the total fault area offsetting the entire suprasalt succession (Table 2). The aspect ratios of normal fault ruptures vary widely (0.4–18); however, most of the observed ruptures are within the range of 0.5 to 3.5 (Nicol et al., 1996; Stock and Smith, 2000), with a mode value of 1.8 (30%; Stock and Smith, 2000). Numerical simulations of strike-slip faults by Weng and Yang (2017) demonstrated that the width of the seismogenic layer significantly influences the rupture aspect ratios. According to their findings, a seismogenic layer thickness of approximately 10 km marks a critical boundary: for thicknesses less than this value, rupture aspect ratios remain low (ca. 2), whereas thicknesses greater than 10 km result in significantly higher aspect ratios (< 8). Considering these findings and given that the suprasalt succession in the southwestern Valencia Trough has an average thickness of approximately 5 km, we adopt an aspect ratio of 1.8 for our calculations.

In the southwestern Valencia Trough, the suprasalt succession thickness at the location of active faults varies. We used thicknesses of 5, 3.3 and 2.3 km for the Cullera, Valencia, and Albufera faults respectively, as input values for our calculation. For events unrestricted by the aspect ratio (i.e., earthquakes rupturing the entire fault length and width of the suprasalt succession), we compute the rupture area as the product of length and width accounting also for the fault dip ($L \times W / \sin \beta$). However, when the seismic potential for ruptures weighted by the aspect ratio is calculated, the controlling factor is the fault width.

The comparison between the standard application of earthquake source scaling relations and the approach presented here for regions characterised by the presence of a weak mechanical layer within the seismogenic crust reveals significant differences (Fig. 12). The maximum expected magnitudes for characteristic events rupturing the entire seismogenic crust (i.e., propagating across the basement–cover interface) are estimated to be 6.9–7.3, 6.4–6.9, and 6.7–7.2 for the Cullera, Valencia, and Albufera Faults, respectively (Table 1). In contrast, for hypothetical earthquakes restricted to the suprasalt succession and rupturing of the total length of the faults, the expected magnitudes are lower, ranging from 6.54–6.96, 5.87–6.48, 6.02–6.59 for the Cullera, Valencia, and Albufera faults, respectively (Table 2). However, in such cases, we argue that the seismic potential derived using area-weighted relations provides a more realistic estimate. Using this approach, our calculations yield maximum magnitudes of 5.79–6.42, 5.42–6.16, and 5.11–5.93 for the Cullera, Valencia, and Albufera faults, respectively (Table 2). These values are 5%–15% lower than those obtained when accounting for the total suprasalt succession thickness.

When the area-weighted values are compared with the maximum expected magnitudes for ruptures involving the entire seismogenic crust, the results reveal a 11%–26% reduction. This discrepancy highlights the importance of incor-

Table 1. Source parameters obtained from length- and area-based scaling relationships (Wells and Coppersmith, 1994 – WC94 – and Stirling et al., 2002 – Stirling02) assuming ruptures involving the entire seismogenic crust. L , fault length; M_w , moment magnitude; AD, average displacement; MD, maximum displacement. Values computed using length-based Wells and Coppersmith (1994) relationships refer to normal faulting (Cullera and Valencia faults) and strike-slip faulting (Albufera Fault).

	Length-based relationships						Area-based relationships		
	WC94			Stirling02			WC94	Stirling02	
	L (km)	M_w	AD (m)	MD (m)	M_w	AD (m)	A (km ²)	M_w	M_w
Cullera Fault	59	7.2 ± 0.34	1.61 ± 0.37	4.94 ± 0.41	7.3 ± 0.30	2.39 ± 0.24	834.4	6.91 ± 0.25	7.22 ± 0.26
Albufera Fault	40	6.97 ± 0.34	0.99 ± 0.37	2.75 ± 0.41	7.16 ± 0.30	2.23 ± 0.24	565.7	6.74 ± 0.25	7.1 ± 0.26
Valencia Fault	20	6.58 ± 0.34	0.42 ± 0.37	0.97 ± 0.41	6.92 ± 0.30	1.97 ± 0.24	282.9	6.43 ± 0.25	6.88 ± 0.26

Table 2. Moment magnitude obtained from scaling relationships (Wells and Coppersmith, 1994 – WC94 – and Stirling et al., 2002 – Stirling02). The first column (not weighted area) corresponds to the values obtained assuming ruptures involving the total suprasalt succession. The second column (weighted area) shows the values obtained using the area weighted by the aspect ratio as input parameter.

	Not weighted area			Weighted area		
	Input parameters A (km ²)	M_w WC94	M_w Stirling02	Input parameters A (km ²)	M_w WC94	M_w Stirling02
	Cullera Fault	360	6.54 ± 0.34	6.96 ± 0.26	67	5.79 ± 0.34
Albufera Fault	112	6.02 ± 0.34	6.59 ± 0.26	14	5.16 ± 0.34	5.93 ± 0.26
Valencia Fault	81	5.87 ± 0.34	6.48 ± 0.26	29	5.42 ± 0.34	6.16 ± 0.26

porating mechanical layering into seismic potential assessments in regions where weak layers influence fault dynamics and rupture propagation. Furthermore, these differences in seismic potential should be addressed in probabilistic seismic hazard assessments.

9 Conclusions

Analysis of a comprehensive subsurface dataset from the southwestern Valencia Trough enables the identification of three major active faults: the normal Cullera Fault, the oblique Albufera Fault, and the normal Valencia Fault. Among these faults, the Cullera Fault is the main active structure in this region, with a cumulative offset of 1800 m at the top of the Messinian marker. The long-term slip rate varies over time between 0.15 ± 0.1 and 0.4 ± 0.1 mm yr⁻¹. The Albufera Fault, which is 55 km in length, has a long-term slip rate of 0.2 ± 0.1 mm yr⁻¹, whereas the 20 km-long Valencia Fault significantly influences the spatial distribution of Quaternary depocentres.

Our results also reveal a 10 km-thick heterogeneous seismogenic crust in the study area, largely because of a mechanically weak layer, which is composed mainly of Triassic evaporites. Consequently, two competing mechanisms are responsible for the offset along the active faults: tectonics and salt withdrawal. A quantitative evolutionary analysis of the

Cullera Fault indicates that tectonics was the dominant mechanism during the Pliocene, whereas salt withdrawal took precedence in the early Quaternary (2.6–2 Ma). After 2 Ma, tectonic activity once again became the primary driver of fault displacement.

Using standard scaling relationships, we computed maximum expected magnitudes for the southwestern Valencia Trough faults. These maximum expected magnitudes range between 6.9–7.3 for the Cullera Fault, 6.7–7.2 for the Albufera Fault, and 6.4–6.9 for de Valencia Fault. However, the mechanically layered crust of the southwestern Valencia Trough influences seismicity: events may nucleate in either the basement or the suprasalt succession. Moreover, the weak layer could influence the vertical propagation of a potential rupture. That is, total or partial decoupling related to the mechanically weak layer implies that an earthquake that nucleated in the suprasalt succession would likely be restricted to this upper part of the seismogenic crust, yet larger events involving basement and cover units are also plausible. For reliable seismic hazard assessments, both scenarios must be accounted for. To compute the seismogenic potential of active faults under the assumption of rupture within the suprasalt succession, we propose the use of the rupture aspect ratio as a correction factor for the maximum rupture area. Specifically, the product of the suprasalt thickness (corrected by the fault dip) and the fault length – weighted by the aspect ratio – provides a more realistic approximation

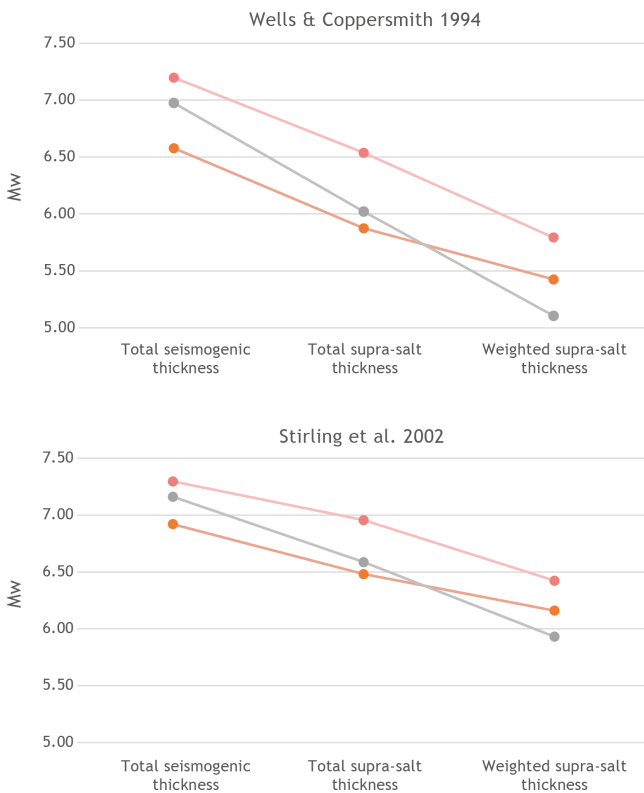


Figure 12. Plots of M_w values for the Cullera, Albufera and Valencia Faults obtained using the scaling relationships of Wells and Coppersmith (1994) and Stirling et al. (2002). The plots show the values computed assuming a rupture of the total seismogenic thickness, a rupture of the total suprasalt succession, and the values assuming a rupture of an area calculated using a suprasalt thickness weighted with the aspect ratio.

of the maximum rupture area. Using this method, the maximum magnitudes for suprasalt ruptures of the southwestern Valencia Trough faults are 5.79–6.42, 5.42–6.16, and 5.11–5.93 for the Cullera, Valencia, and Albufera faults, respectively. These values are 5%–15% lower than those obtained by considering the full suprasalt thickness alone, and 11%–26% lower than estimates involving the entire seismogenic crust.

Overall, these findings greatly enhance our understanding of the seismogenic potential of the southwestern Valencia Trough, an offshore area near densely populated areas. These findings provide a basis for improved seismic hazard assessments. Additionally, as we are addressing offshore faults exhibiting vertical displacement, our findings can be used to establish the tsunamigenic potential of this region. Furthermore, this approach for incorporating mechanical heterogeneities in the seismogenic crust can be applied to other regions and tectonic settings with analogous structural configurations.

Code availability. The authors acknowledge the use of the MOVE Software Suite granted by PE Limited (Petex). MOVE can be obtained at <https://www.petex.com/> (last access: 11 May 2026).

Data availability. Vintage 2D seismic reflection profiles acquired during the late 1970s by various operators were used in this study. These seismic data are publicly available upon request from the Instituto Geológico y Minero de España (IGME-CSIC) through the SIGEOF database (<http://info.igme.es/sigeof>, last access: 11 May 2026).

Original well reports, wireline log data (including lithological descriptions, dipmeter, gamma-ray, sonic and resistivity logs), and palaeontological data derived from cuttings and sidewall cores were retrieved from the hydrocarbon exploration archives of the Instituto Geológico y Minero de España (IGME-CSIC) (<https://info.igme.es/hidrocarburos>, last access: 11 May 2026).

Additional stratigraphic and hydrogeological information was obtained from 95 hydrogeological wells located in the Valencia coastal plain, together with vertical electrical sounding (VES) data acquired for hydrogeological surveys. These datasets are publicly accessible through the online databases IRYDA, BD Puntos Agua 2.0 and Sistema de Información Documental (SID), hosted by the Instituto Geológico y Minero de España (IGME-CSIC) and available via the institutional catalogue (<https://info.igme.es/catalogo>, last access: 11 May 2026).

Author contributions. IMR: Conceptualization, Data curation, Formal analysis, Funding acquisition, Investigation, Methodology, Project administration, Supervision, Validation, Visualization, Writing – original draft preparation, review & editing. AR: Data curation, Formal analysis, Funding acquisition, Investigation, Resources, Visualization, Writing – original draft preparation, review & editing. MDR: Data curation, Formal analysis, Investigation, Resources, Visualization, Writing – original draft preparation, review & editing. IMC: Data curation, Formal analysis, Investigation, Visualization, Writing –review & editing. ESP: Data curation, Formal analysis, Investigation, Writing –review & editing. PA: Data curation, Formal analysis, Investigation, Supervision, Writing –review & editing.

Competing interests. The contact author has declared that none of the authors has any competing interests.

Disclaimer. Publisher's note: Copernicus Publications remains neutral with regard to jurisdictional claims made in the text, published maps, institutional affiliations, or any other geographical representation in this paper. The authors bear the ultimate responsibility for providing appropriate place names. Views expressed in the text are those of the authors and do not necessarily reflect the views of the publisher.

Acknowledgements. We acknowledge the comments of the Raúl Pérez-López, two anonymous reviewers, and the Editor Solmaz Mohadjer, which significantly improved the quality of this paper.

Financial support. This research was funded by the Spanish Ministry of Science, Innovation and University (research projects PID2021-127967NB-I00 and RTI2018-100737-B-I00), Generalitat Valenciana (Valencian Regional Government, research projects AICO2021/196 and CIAPOS/2022/082), and University of Alicante (research project VIGROB053).

Review statement. This paper was edited by Solmaz Mohadjer and reviewed by Raul Perez-Lopez and two anonymous referees.

References

- Albarracín, S., Alcántara-Carrió, J., Barranco, A., Sánchez García, M. J., Fontán Bouzas, Á., and Rey Salgado, J.: Seismic evidence for the preservation of several stacked Pleistocene coastal barrier/lagoon systems on the Gulf of Valencia continental shelf (western Mediterranean), *Geo-Mar. Lett.*, 33, 217–223, <https://doi.org/10.1007/s00367-012-0315-x>, 2013.
- Arche, A. and López-Gómez, J.: Origin of the Permian-Triassic Iberian Basin, central-eastern Spain, *Tectonophysics*, 266, 443–464, [https://doi.org/10.1016/S0040-1951\(96\)00202-8](https://doi.org/10.1016/S0040-1951(96)00202-8), 1996.
- Arche, A., Evans, G., and Clavell, E.: Some considerations on the initiation of the present SE Ebro river drainage system: Post- or pre-Messinian?, *J. Iber. Geol.*, 36, 73–85, 2010.
- Barchi, M. R. and Mirabella, F.: The 1997–98 Umbria–Marche earthquake sequence: “Geological” vs. “seismological” faults, *Tectonophysics*, 476, 170–179, <https://doi.org/10.1016/j.tecto.2008.09.013>, 2009.
- Barchi, M. R., Carboni, F., Michele, M., Ercoli, M., Giorgetti, C., Porreca, M., Azzaro, S., and Chiaraluze, L.: The influence of subsurface geology on the distribution of earthquakes during the 2016–2017 Central Italy seismic sequence, *Tectonophysics*, 807, 228797, <https://doi.org/10.1016/j.tecto.2021.228797>, 2021.
- Boncio, P., Lavecchia, G., and Pace, B.: Defining a model of 3D seismogenic sources for seismic hazard assessment applications: The case of central Apennines (Italy), *J. Seismol.*, 8, 407–425, <https://doi.org/10.1023/B:JOSE.0000038449.78801.05>, 2004.
- Bufo, E. and Udías, A.: The 1620 and 1644 Earthquakes in Alcoy and the Eastern Region of Spain, *Seismol. Res. Lett.*, 93, 2335–2346, <https://doi.org/10.1785/0220220053>, 2022.
- Bufo, E., Udías, A., Sanz de Galdeano, C., and Cesca, S.: The 1748 Montesa (southeast Spain) earthquake – A singular event, *Tectonophysics*, 664, 139–153, <https://doi.org/10.1016/j.tecto.2015.09.005>, 2015.
- Cameselle, A. L. and Urgeles, R.: Large-scale margin collapse during Messinian early sea-level drawdown: the SW Valencia trough, NW Mediterranean, *Basin Res.*, 29, 576–595, <https://doi.org/10.1111/bre.12170>, 2017.
- Cameselle, A. L., Urgeles, R., De Mol, B., Camerlenghi, A., and Canning, J. C.: Late Miocene sedimentary architecture of the Ebro Continental Margin (Western Mediterranean): implications to the Messinian Salinity Crisis, *Int. J. Earth Sci.*, 103, 423–440, <https://doi.org/10.1007/s00531-013-0966-5>, 2014.
- Centamore, E., Adamoli, L., Berti, D., Bigi, G., Bigi, S., Casnedi, R., Cantalamessa, R., Fumanti, G., Morelli, F., Micarelli, C., Ridolfi, A., and Salvucci, M.: Carta geologica dei bacini della Laga e del Cellino e dei rilievi carbonatici circostanti, in *Studi Geologici Camerti*, Vol. Università degli Studi, Dipartimento di Scienze della Terra, SELCA, Firenze, 1992.
- Cheng, J., Rong, Y., Magistrale, H., Chen, G., and Xu, X.: Earthquake rupture scaling relations for mainland China, *Seismol. Res. Lett.*, 91, 248–261, <https://doi.org/10.1785/0220190129>, 2019.
- Chiaraluze, L., Ellsworth, W. L., Chiarabba, C., and Cocco, M.: Imaging the complexity of an active normal fault system: The 1997 Colfiorito (central Italy) case study, *J. Geophys. Res.-Sol. Ea.*, 108, <https://doi.org/10.1029/2002JB002166>, 2003.
- Chiaraluze, L., Di Stefano, R., Tinti, E., Scognamiglio, L., Michele, M., Casarotti, E., Cattaneo, M., De Gori, P., Chiarabba, C., Monachesi, G., Lombardi, A., Valoroso, L., Latorre, D., and Marzorati, S.: The 2016 Central Italy seismic sequence: a first look at the mainshocks, aftershocks, and source models, *Seismol. Res. Lett.*, 88, 757–771, <https://doi.org/10.1785/0220160221>, 2017.
- Clavell, E. and Berástegui, X.: Petroleum geology of the Gulf of Valencia, in: *Generation, Accumulation and Production of Europe’s Hydrocarbons*, edited by: Spencer, A. M., Special Publication of the European Association of Petroleum Geoscientists, 1, Oxford University Press, Oxford, 355–368, ISBN 978-0198542827, 1991.
- Cresta, S., Monechi, S., Parisi, G., Baldanza, A., and Reale, V.: Mesozoic-Cenozoic Stratigraphy in the Umbria–Marche Area: Geological Field Trips in the Umbria–Marche Apennines (Italy), *Memorie Descrittive Della Carta Geologica d’Italia*, 39, 185, ISBN 978-88-240-2295-5, 1989.
- DeMets, C., Gordon, R. G., Argus, D. F., and Stein, S.: Effect of recent revisions to the geomagnetic reversal time scale on estimates of current plate motions, *Geophys. Res. Lett.*, 21, 2191–2194, <https://doi.org/10.1029/94GL02118>, 1994.
- De Ruig, M. J.: Tectono-sedimentary evolution of the Prebetic fold belt of Alicante, PhD thesis, Vrije Universiteit Amsterdam, 207 pp., ISBN 9090052348, 1992.
- De Ruig, M. J.: Extensional diapirism in the eastern Prebetic fold-belt, southeastern Spain, in: *Salt Tectonics: A Global Perspective*, edited by: Jackson, M. P. A., Roberts, D. G., and Snelson, S., AAPG Memoir, 65, American Association of Petroleum Geologists, 353–367, <https://doi.org/10.1306/M65604C17>, 1995.
- Díaz del Río, V., Rey, J., and Vegas, R.: The Gulf of Valencia continental shelf: Extensional tectonics in Neogene and Quaternary sediments, *Mar. Geol.*, 73, 169–179, [https://doi.org/10.1016/0025-3227\(86\)90117-9](https://doi.org/10.1016/0025-3227(86)90117-9), 1986.
- Duffy, O. B., Gawthorpe, R. L., and Docherty, M.: Tectono-stratigraphic evolution of salt-influenced normal fault systems: an example from the Coffee-Soil Fault, Danish North Sea, *J. Geol. Soc.*, 180, 1, <https://doi.org/10.1144/jgs2023-016>, 2023.
- Etheve, N., Frizon de Lamotte, D., Mohn, G., Martos, R., Roca, E., and Blanpied, C.: Extensional vs contractional Cenozoic deformation in Ibiza (Balearic Promontory, Spain): Integration in the West Mediterranean back-arc setting, *Tectonophysics*, 682, 35–55, <https://doi.org/10.1016/j.tecto.2016.05.037>, 2016.
- Etheve, N., Mohn, G., Frizon de Lamotte, D., Roca, E., Tugend, J., and Gómez-Romeu, J.: Extreme Mesozoic Crustal Thinning in the Eastern Iberia Margin: The Example of the Columbrets Basin (Valencia Trough), *Tectonics*, 37, 636–662, <https://doi.org/10.1002/2017TC004613>, 2018.
- Faccenna, C., Piromallo, C., Crespo-Blanc, A., Jolivet, L., and Rossetti, F.: Lateral slab deformation and the ori-

- gin of the western Mediterranean arcs, *Tectonics*, 23, <https://doi.org/10.1029/2002TC001488>, 2004.
- Fang, P., Tugend, J., Mohn, G., Kuszniir, N., and Ding, W.: Evidence for rapid large-amplitude vertical motions in the Valencia Trough (Western Mediterranean) generated by 3D subduction slab roll-back, *Earth Planet. Sc. Lett.*, 575, 117179, <https://doi.org/10.1016/j.epsl.2021.117179>, 2021.
- Ford, M., Le Carlier de Veslud, C., and Bourgeois, O.: Kinematic and geometric analysis of fault-related folds in a rift setting: The Dannemarie basin, Upper Rhine Graben, France, *J. Struct. Geol.*, 29, 1811–1830, <https://doi.org/10.1016/j.jsg.2007.08.001>, 2007.
- García-Mayordomo, J.: Caracterización y análisis de la peligrosidad sísmica en el sureste de España, PhD thesis, Universidad Complutense de Madrid, 379 pp., <https://www.fundaciongarciasineriz.es/wp-content/uploads/attachments/JGarcia.pdf> (last access: 11 May 2026), 2012.
- García-Mayordomo, J., Insua-Arévalo, J. M., Martínez-Díaz, J. J., Jiménez-Díaz, A., Martín-Banda, R., Martín-Alfageme, S., Álvarez-Gómez, J. A., Rodríguez-Peces, M., Pérez-López, R., Rodríguez-Pascua, M. A., Masana, E., Perea, H., Martín-González, F., Giner-Robles, J., Nemser, E. S., and Cabral, J.: The Quaternary active faults database of Iberia (QAFI v. 2.0), *J. Iber. Geol.*, 38, https://doi.org/10.5209/rev_JIGE.2012.v38.n1.39219, 2012.
- Gaspar-Escribano, J. M., Garcia-Castellanos, D., Roca, E., and Cloetingh, S.: Cenozoic vertical motions of the Catalan Coastal Ranges (NE Spain): The role of tectonics, isostasy, and surface transport, *Tectonics*, 23, <https://doi.org/10.1029/2003TC001511>, 2004.
- Geel, T.: Oligocene to early Miocene tectono-sedimentary history of the Alicante region (SE Spain): implications for Western Mediterranean evolution, *Basin Res.*, 7, 313–336, <https://doi.org/10.1111/j.1365-2117.1995.tb00120.x>, 1995.
- Geller, R. J.: Scaling relations for earthquake source parameters and magnitudes, *B. Seismol. Soc. Am.*, 66, 1501–1523, 1976.
- Getech: Global Gravity and Magnetic Data, <https://getech.com/> (last access: 11 May 2026), 2015.
- Godano, C., Convertito, V., Tramelli, A., and Petrillo, G.: Interplay between ground deformation and seismicity during the 2005–2025 unrest at Campi Flegrei, *Sci. Rep.*, 15, 43238, <https://doi.org/10.1038/s41598-025-27259-4>, 2025.
- González, Á.: The Spanish National Earthquake Catalogue: Evolution, precision and completeness, *J. Seismol.*, 21, 435–471, <https://doi.org/10.1007/s10950-016-9610-8>, 2017.
- Guimerà, J. and Álvaro, M.: Structure et évolution de la compression alpine dans la Chaîne ibérique et la Chaîne côtière catalane (Espagne), *B. Soc. Géol. Fr.*, 6, 339–348, <https://doi.org/10.2113/gssgfbull.VI.2.339>, 1990.
- Hongxing, G. and Anderson, J. K.: Fault throw profile and kinematics of normal fault: conceptual models and geologic examples, *Geological Journal of China Universities*, 13, 75–88, 2007.
- Huang, J., Abrahamson, N. A., Sung, C., and Chao, S.: New empirical source-scaling laws for crustal earthquakes incorporating fault dip and seismogenic-thickness effects, *Seismol. Res. Lett.*, 95, 2352–2367, <https://doi.org/10.1785/0220240034>, 2024.
- Hyndman, R. D., Yamano, M., and Oleskevich, D. A.: The seismogenic zone of subduction thrust faults, *Island Arc*, 6, 244–260, <https://doi.org/10.1111/j.1440-1738.1997.tb00175.x>, 1997.
- IGN: Servicio de Información Sísmica, Instituto Geográfico Nacional, <https://www.ign.es/web/ign/portal/sis-area-sismicidad> (last access: 15 March 2025), 2025.
- Improta, L., Latorre, D., Margheriti, L., Nardi, A., Marchetti, A., Lombardi, A. M., Castello, B., Villani, F., Ciaccio, M. G., Mele, F. M., Moretti, M., Battelli, P., Berardi, M., Castellano, C., Melorio, C., Modica, G., Pirro, M., Rossi, A., Thermes, C., and Di Maro, R.: Multi-segment rupture of the 2016 Amatrice-Visso-Norcia seismic sequence (central Italy) constrained by the first high-quality catalog of early aftershocks, *Sci. Rep.*, 9, 6921, <https://doi.org/10.1038/s41598-019-43393-2>, 2019.
- Jackson, C. A.-L. and Rotevatn, A.: 3D seismic analysis of the structure and evolution of a salt-influenced normal fault zone: A test of competing fault growth models, *J. Struct. Geol.*, 54, 215–234, <https://doi.org/10.1016/j.jsg.2013.06.012>, 2013.
- Jackson, M. P. A. and Hudec, M. R.: Stratigraphic record of translation down ramps in a passive-margin salt detachment, *J. Struct. Geol.*, 27, 889–911, <https://doi.org/10.1016/j.jsg.2005.01.010>, 2005.
- Jolivet, L. and Faccenna, C.: Mediterranean extension and the Africa-Eurasia collision, *Tectonics*, 19, 1095–1106, <https://doi.org/10.1029/2000TC900018>, 2000.
- Kanamori, H. and Anderson, D. L.: Theoretical basis of some empirical relations in seismology, *B. Seismol. Soc. Am.*, 65, 1073–1095, 1975.
- Kane, K. E., Jackson, C. A.-L., and Larsen, E.: Normal fault growth and fault-related folding in a salt-influenced rift basin: South Viking Graben, offshore Norway, *J. Struct. Geol.*, 32, 490–506, <https://doi.org/10.1016/j.jsg.2010.02.005>, 2010.
- Lanaja, J. M.: Contribución de la exploración petrolífera al conocimiento de la geología de España, Instituto Geológico y Minero de España (IGME), Madrid, ISBN 978-84-7474-398-2, 1987.
- Leonard, M.: Earthquake fault scaling; self-consistent relating of rupture length, width, average displacement, and moment release, *B. Seismol. Soc. Am.*, 100, 1971–1988, <https://doi.org/10.1785/0120090189>, 2010.
- Leonard, M.: Self-consistent earthquake fault-scaling relations; update and extension to stable continental strike-slip faults, *B. Seismol. Soc. Am.*, 104, 2953–2965, <https://doi.org/10.1785/0120140087>, 2014.
- Lirer, F., Foresi, L. M., Iaccarino, S. M., Salvatorini, G., Turco, E., Cosentino, C., Sierro, F. J., and Caruso, A.: Mediterranean Neogene planktonic foraminifer biozonation and biochronology, *Earth-Sci. Rev.*, 196, 102869, <https://doi.org/10.1016/j.earscirev.2019.05.013>, 2019.
- Lofi, J., Déverchère, J., Gaullier, V., Gillet, H., Gorini, C., Guennoc, P., Loncke, L., Maillard, A., Sage, F., and Thinon, I.: Seismic atlas of the “Messinian Salinity Crisis” markers in the Mediterranean and Black Seas, Commission for the Geological Map of the World and Mémoires de la Société Géologique de France, Nouvelle Série, 72 pp., 2011.
- Maillard, A. and Mauffret, A.: Crustal structure and rifting of the Valencia Trough (north-western Mediterranean Sea), *Basin Res.*, 11, 357–379, <https://doi.org/10.1046/j.1365-2117.1999.00105.x>, 1999.
- Maillard, A. and Mauffret, A.: Structure and present-day compression in the offshore area between Alicante and Ibiza Is-

- land (Eastern Iberian Margin), *Tectonophysics*, 591, 116–130, <https://doi.org/10.1016/j.tecto.2011.07.007>, 2013.
- Maillard, A., Mauffret, A., Watts, A. B., Torné, M., Pascal, G., Buhl, P., and Pinet, B.: Tertiary sedimentary history and structure of the Valencia trough (western Mediterranean), *Tectonophysics*, 203, 57–75, [https://doi.org/10.1016/0040-1951\(92\)90215-R](https://doi.org/10.1016/0040-1951(92)90215-R), 1992.
- Mancilla, F. d. L., Stich, D., Morales, J., Martín, R., Diaz, J., Pazos, A., Córdoba, D., Pulgar, J. A., Ibarra, P., Harnafi, M., and Gonzalez-Lodeiro, F.: Crustal thickness and images of the lithospheric discontinuities in the Gibraltar arc and surrounding areas, *Geophys. J. Int.*, 203, 1804–1820, <https://doi.org/10.1093/gji/ggv390>, 2015.
- Mansfield, C. S. and Cartwright, J. A.: High resolution fault displacement mapping from three-dimensional seismic data: evidence for dip linkage during fault growth, *J. Struct. Geol.*, 18, 249–263, [https://doi.org/10.1016/S0191-8141\(96\)80048-4](https://doi.org/10.1016/S0191-8141(96)80048-4), 1996.
- Marsh, N., Imber, J., Holdsworth, R. E., Brockbank, P., and Ringrose, P.: The structural evolution of the Halten Terrace, offshore Mid-Norway: extensional fault growth and strain localisation in a multi-layer brittle-ductile system, *Basin Res.*, 22, 195–214, <https://doi.org/10.1111/j.1365-2117.2009.00404.x>, 2010.
- Martí, J., Mitjavila, J., Roca, E., and Aparicio, A.: Cenozoic magmatism of the Valencia Trough (western Mediterranean): Relationship between structural evolution and volcanism, *Tectonophysics*, 203, 145–165, [https://doi.org/10.1016/0040-1951\(92\)90221-Q](https://doi.org/10.1016/0040-1951(92)90221-Q), 1992.
- Martínez-Solares, J. M. and Mezcuca, J.: Catálogo sísmico de la Península Ibérica, Instituto Geográfico Nacional, Madrid, <https://www.ign.es/web/resources/docs/IGNCnig/SIS-Catalogo-hasta-1900.pdf> (last access: 11 May 2026), 2002.
- Martinis, B. and Pieri, M.: Alcune notizie sulla formazione evaporitica del Triassico Superiore nell'Italia centrale e meridionale, *Memorie della Società Geologica Italiana*, 4, 649–678, 1964.
- Maurin, J. and Nivière, B.: Extensional forced folding and décollement of the pre-rift series along the Rhine graben and their influence on the geometry of the syn-rift sequences, in: *Forced Folds and Fractures*, Geological Society, London, Special Publications, 73–86, <https://doi.org/10.1144/GSL.SP.2000.169.01.06>, 1999.
- McClusky, S., Reilinger, R., Mahmoud, S., Ben Sari, D., and Tealeb, A.: GPS constraints on Africa (Nubia) and Arabia plate motions, *Geophys. J. Int.*, 155, 126–138, <https://doi.org/10.1046/j.1365-246X.2003.02023.x>, 2003.
- Menichetti, M. and Coccioni, R.: Umbria – Marche Apennines geological field trip, 2013, *Livret – Guide des Excursions du Groupe Français du Crétacé*, https://hal.science/hal-01236473v1/file/excursion_GFC_2013.pdf (last access: 11 May 2026), 2013.
- Michele, M., Chiaraluce, L., Di Stefano, R., and Waldhauser, F.: Fine-scale structure of the 2016–2017 Central Italy seismic sequence from data recorded at the Italian National Network, *J. Geophys. Res.-Sol. Ea.*, 125, <https://doi.org/10.1029/2019JB018440>, 2020.
- Morley, C. K., Back, S., Van Rensbergen, P., Crevello, P., and Lambiase, J. J.: Characteristics of repeated, detached, Miocene–Pliocene tectonic inversion events, in a large delta province on an active margin, Brunei Darussalam, Borneo, *J. Struct. Geol.*, 25, 1147–1169, [https://doi.org/10.1016/S0191-8141\(02\)00130-X](https://doi.org/10.1016/S0191-8141(02)00130-X), 2003.
- Nebot, M. and Guimerà, J.: Kinematic evolution of a fold-and-thrust belt developed during basin inversion: the Mesozoic Maestrat basin, E Iberian Chain, *Geol. Mag.*, 155, 630–640, <https://doi.org/10.1017/S001675681600090X>, 2018.
- Nicol, A., Watterson, J., Walsh, J. J., and Childs, C.: The shapes, major axis orientations and displacement patterns of fault surfaces, *J. Struct. Geol.*, 18, 235–248, [https://doi.org/10.1016/S0191-8141\(96\)80047-2](https://doi.org/10.1016/S0191-8141(96)80047-2), 1996.
- Nocquet, J.-P.: Present-day kinematics of the Mediterranean: A comprehensive overview of GPS results, *Tectonophysics*, 579, 220–242, <https://doi.org/10.1016/j.tecto.2012.03.037>, 2012.
- Nocquet, J.-P. and Calais, E.: Crustal velocity field of western Europe from permanent GPS array solutions, 1996–2001, *Geophys. J. Int.*, 154, 72–88, <https://doi.org/10.1046/j.1365-246X.2003.01935.x>, 2003.
- Palano, M., González, P. J., and Fernández, J.: The diffuse plate boundary of Nubia and Iberia in the Western Mediterranean: Crustal deformation evidence for viscous coupling and fragmented lithosphere, *Earth Planet. Sc. Lett.*, 430, 439–447, <https://doi.org/10.1016/j.epsl.2015.08.040>, 2015.
- Palomeras, I., Villaseñor, A., Thurner, S., Levander, A., Gallart, J., and Harnafi, M.: Lithospheric structure of Iberia and Morocco using finite-frequency Rayleigh wave tomography from earthquakes and seismic ambient noise: Rayleigh Wave Tomography In WM, *Geochem. Geophys. Geosyst.*, 18, 1824–1840, <https://doi.org/10.1002/2016GC006657>, 2017.
- Pascal, G., Torné, M., Buhl, P., Watts, A. B., and Mauffret, A.: Crustal and velocity structure of the Valencia trough (western Mediterranean), Part II. Detailed interpretation of five Expanded Spread Profiles, *Tectonophysics*, 203, 21–35, [https://doi.org/10.1016/0040-1951\(92\)90213-P](https://doi.org/10.1016/0040-1951(92)90213-P), 1992.
- Pascoe, R., Hooper, R., Storhaug, K., and Harper, H.: Evolution of extensional styles at the southern termination of the Nordland Ridge, Mid-Norway: a response to variations in coupling above Triassic salt, *Petroleum Geology Conference Series*, 5, 83–90, <https://doi.org/10.1144/0050083>, 1999.
- Perea, H.: Falles actives i perillositat sísmica al marge nord-occidental del solc de València, PhD thesis, Universitat de Barcelona, 382 pp., ISBN 9788469037690, 2006.
- Pérez-Peña, A., Martín-Davila, J., Gárate, J., Berrocoso, M., and Buforn, E.: Velocity field and tectonic strain in Southern Spain and surrounding areas derived from GPS episodic measurements, *J. Geodyn.*, 49, 232–240, <https://doi.org/10.1016/j.jog.2010.01.015>, 2010.
- Ramos, A., Lopez-Mir, B., Wilson, E. P., Granado, P., and Muñoz, J. A.: 3D reconstruction of syn-tectonic strata in a salt-related orogen: learnings from the Lleret syncline (South-central Pyrenees), *Geol. Acta*, 18, 1–19, <https://doi.org/10.1344/GeologicaActa2020.18.20>, 2020.
- Ramos, A., Pedrera, A., García-Senz, J., López-Mir, B., and Salas, R.: Seismic evidence for ductile necking of the mid-lower crust beneath the Columbrets Basin (Western Mediterranean), *Terra Nova*, 35, 404–412, <https://doi.org/10.1111/ter.12664>, 2023.
- Ramos, A., de Ruig, M. J., Pedrera, A., Alfaro, P., and Martin-Rojas, I.: Salt expulsion triggered by prograding clinoforms in the SW Valencia Trough (SE Spain), *Mar. Petrol. Geol.*, 173, 107268, <https://doi.org/10.1016/j.marpetgeo.2024.107268>, 2025.

- Rehault, J., Boillot, G., and Mauffret, A.: The Western Mediterranean Basin geological evolution, *Mar. Geol.*, 55, 447–477, [https://doi.org/10.1016/0025-3227\(84\)90081-1](https://doi.org/10.1016/0025-3227(84)90081-1), 1984.
- Ribó, M., Puig, P., Muñoz, A., Lo Iacono, C., Masqué, P., Palanques, A., Acosta, J., Guillén, J., and Gómez Ballesteros, M.: Morphobathymetric analysis of the large fine-grained sediment waves over the Gulf of Valencia continental slope (NW Mediterranean), *Geomorphology*, 253, 22–37, <https://doi.org/10.1016/j.geomorph.2015.09.027>, 2016a.
- Ribó, M., Puig, P., Urgeles, R., Van Rooij, D., and Muñoz, A.: Spatio-temporal evolution of sediment waves developed on the Gulf of Valencia margin (NW Mediterranean) during the Plio-Quaternary, *Mar. Geol.*, 378, 276–291, <https://doi.org/10.1016/j.margeo.2015.11.011>, 2016b.
- Richardson, N. J., Underhill, J. R., and Lewis, G.: The role of evaporite mobility in modifying subsidence patterns during normal fault growth and linkage, Halten Terrace, Mid-Norway, *Basin Res.*, 17, 203–223, <https://doi.org/10.1111/j.1365-2117.2005.00250.x>, 2005.
- Roca, E.: L'estructura de la conca Catalano-Balear: paper de la compressió i de la distensió en la seva gènesi, PhD Thesis, Universitat de Barcelona, 330 pp., <https://hdl.handle.net/2445/34919> (last access: 11 May 2026), 1992.
- Roca, E.: La evolución geodinámica de la Cuenca Catalano-Baleary áreas adyacentes desde el Mesozoico hasta la actualidad, *Acta Geologica Hispanica*, 29, 3–25, 1996.
- Roca, E.: The Northwest-Mediterranean basin (Valencia Trough, Gulf of Lions and Liguro-Provençal basins): structure and geodynamic evolution, in: Peri-Tethyan Rift/Wrench Basins and Passive Margins, edited by: Ziegler, P. A., Cavazza, W., Robertson, A. F. H., and Crasquin-Soleau, S., *Mémoires du Muséum National d'Histoire Naturelle*, 186, 671–706, 2001.
- Roca, E. and Desegaulx, P.: Analysis of the geological evolution and vertical movements in the València Trough area, western Mediterranean, *Mar. Petrol. Geol.*, 9, 167–185, [https://doi.org/10.1016/0264-8172\(92\)90089-W](https://doi.org/10.1016/0264-8172(92)90089-W), 1992.
- Roca, E. and Guimerà, J.: The Neogene structure of the eastern Iberian margin: Structural constraints on the crustal evolution of the Valencia trough (western Mediterranean), *Tectonophysics*, 203, 203–218, [https://doi.org/10.1016/0040-1951\(92\)90224-T](https://doi.org/10.1016/0040-1951(92)90224-T), 1992.
- Roca, E., Sans, M., Cabrera, L., and Marzo, M.: Oligocene to Middle Miocene evolution of the central Catalan margin (northwestern Mediterranean), *Tectonophysics*, 315, 209–229, [https://doi.org/10.1016/S0040-1951\(99\)00289-9](https://doi.org/10.1016/S0040-1951(99)00289-9), 1999.
- Roca, E., Frizon de Lamotte, D., Mauffret, A., Bracene, R., Verges, J., Benaouali, N., Fernandez, M., Muñoz, J. A., and Zeyen, H.: TRANSMED-transect II (Aquitaine basin, Pyrenees, Ebro basin, Catalan Coastal Ranges, Valencia Trough, Balearic Promontory, Algerian Basin, Tell, Sahara Atlas, Sahara Platform), in: The TRANSMED Atlas – The Mediterranean Region from Crust to Mantle, edited by: Cavazza, W., Roure, F., Spakman, W., Stampfli, G. M., and Ziegler, P. A., Springer, Berlin, Heidelberg, 2004.
- Roma, M., Ferrer, O., Roca, E., Pla, O., Escosa, F. O., and Butillé, M.: Formation and inversion of salt-detached ramp-syncline basins. Results from analog modeling and application to the Columbrets Basin (Western Mediterranean), *Tectonophysics*, 745, 214–228, <https://doi.org/10.1016/j.tecto.2018.08.012>, 2018.
- Rouby, D., Guillocheau, F., Robin, C., Bouroulec, R., Railroad, S., Castellort, S., and Nalpas, T.: Rates of deformation of an extensional growth fault/raft system (offshore Congo, West African margin) from combined accommodation measurements and 3-D restoration, *Basin Res.*, 15, 183–200, <https://doi.org/10.1046/j.1365-2117.2003.00200.x>, 2003.
- Rovida, A., Locati, M., Camassi, R., Lolli, B., and Gasperini, P.: The Italian earthquake catalogue CPTI15, *B. Earthq. Eng.*, 18, 2953–2984, <https://doi.org/10.1007/s10518-020-00818-y>, 2020.
- Ruff, L. and Kanamori, H.: Seismic coupling and uncoupling at subduction zones, *Tectonophysics*, 99, 99–117, [https://doi.org/10.1016/0040-1951\(83\)90097-5](https://doi.org/10.1016/0040-1951(83)90097-5), 1983.
- Sàbat, F., Gelabert, B., Rodríguez-Perea, A., and Giménez, J.: Geological structure and evolution of Majorca: Implications for the origin of the Western Mediterranean, *Tectonophysics*, 510, 217–238, <https://doi.org/10.1016/j.tecto.2011.07.005>, 2011.
- Salas, R., Guimerà, J., Mas, R., Martín-Closas, C., Melendez, A., and Alonso, A.: Evolution of the Mesozoic Central Iberian Rift System and its Cainozoic inversion (Iberian chain), in: Peri-Tethyan Rift/Wrench Basins and Passive Margins, edited by: Ziegler, P. A., Cavazza, W., Robertson, A. F. H., and Crasquin-Soleau, S., *Mémoires du Muséum National d'Histoire Naturelle*, 186, 145–186, 2001.
- Séranne, M.: The Gulf of Lion continental margin (NW Mediterranean) revisited by IBS: an overview, in: Geological Society, London, Special Publications, 15–36, <https://doi.org/10.1144/GSL.SP.1999.156.01.03>, 1999.
- Serpelloni, E., Vannucci, G., Pondrelli, S., Argnani, A., Casula, G., Anzidei, M., Baldi, P., and Gasperini, P.: Kinematics of the Western Africa-Eurasia plate boundary from focal mechanisms and GPS data, *Geophys. J. Int.*, 169, 1180–1200, <https://doi.org/10.1111/j.1365-246X.2007.03367.x>, 2007.
- Soler y José, R., Martínez del Olmo, W., Megías, A. G., and Abeger Montegudo, J. A.: Rasgos básicos del neógeno del Mediterráneo español, *Mediterránea. Serie de Estudios Geológicos*, 1, 71–82, 1983.
- Stampfli, G. M. and Höcker, C. F. W.: Messinian palaeorelief from a 3-D seismic survey in the Tarraco concession area (Spanish Mediterranean Sea), *Geol. Mijnbouw*, 68, 201–210, 1989.
- Stewart, S. A., Ruffell, A. H., and Harvey, M. J.: Relationship between basement-linked and gravity-driven fault systems in the UKCS salt basins, *Mar. Petrol. Geol.*, 14, 581–604, [https://doi.org/10.1016/S0264-8172\(97\)00008-1](https://doi.org/10.1016/S0264-8172(97)00008-1), 1997.
- Stich, D., Serpelloni, E., de Lis Mancilla, F., and Morales, J.: Kinematics of the Iberia–Maghreb plate contact from seismic moment tensors and GPS observations, *Tectonophysics*, 426, 295–317, <https://doi.org/10.1016/j.tecto.2006.08.004>, 2006.
- Stich, D., Martín, R., and Morales, J.: Moment tensor inversion for Iberia–Maghreb earthquakes 2005–2008, *Tectonophysics*, 483, 390–398, <https://doi.org/10.1016/j.tecto.2009.11.006>, 2010.
- Stirling, M., Rhoades, D., and Berryman, K.: Comparison of earthquake scaling relations derived from data of the instrumental and preinstrumental era, *B. Seismol. Soc. Am.*, 92, 812–830, <https://doi.org/10.1785/0120000221>, 2002.
- Stirling, M., Goded, T., Berryman, K., and Litchfield, N.: Selection of earthquake scaling relationships for seismic-hazard analysis, *B. Seismol. Soc. Am.*, 103, 2993–3011, <https://doi.org/10.1785/0120130052>, 2013.

- Stock, C. and Smith, E. G. C.: Evidence for different scaling of earthquake source parameters for large earthquakes depending on faulting mechanism, *Geophys. J. Int.*, 143, 157–162, <https://doi.org/10.1046/j.1365-246x.2000.00225.x>, 2000.
- Thorsen, C. E.: Age of growth faulting in southeast Louisiana, *Transactions of the Gulf Coast Association of Geological Societies*, 13, 103–110, 1963.
- Torné, M., Pascal, G., Buhl, P., Watts, A. B., and Mauffret, A.: Crustal and velocity structure of the Valencia trough (western Mediterranean), Part I. A combined refraction/wide-angle reflection and near-vertical reflection study, *Tectonophysics*, 203, 1–20, [https://doi.org/10.1016/0040-1951\(92\)90212-O](https://doi.org/10.1016/0040-1951(92)90212-O), 1992.
- Tvedt, A. B. M., Rotevatn, A., Jackson, C. A.-L., Fossen, H., and Gawthorpe, R. L.: Growth of normal faults in multi-layer sequences: A 3D seismic case study from the Egersund Basin, Norwegian North Sea, *J. Struct. Geol.*, 55, 1–20, <https://doi.org/10.1016/j.jsg.2013.08.002>, 2013.
- Valoroso, L., Chiaraluce, L., Piccinini, D., Di Stefano, R., Schaff, D., and Waldhauser, F.: Radiography of a normal fault system by 64 000 high-precision earthquake locations: The 2009 L'Aquila (central Italy) case study, *J. Geophys. Res.-Sol. Ea.*, 118, 1156–1176, <https://doi.org/10.1002/jgrb.50130>, 2013.
- van Hinsbergen, D. J. J., Vissers, R. L. M., and Spakman, W.: Origin and consequences of western Mediterranean subduction, rollback, and slab segmentation, *Tectonics*, 33, 393–419, <https://doi.org/10.1002/2013TC003349>, 2014.
- Vargas, H., Gaspar-Escribano, J. M., López-Gómez, J., Van Wees, J., Cloetingh, S., de La Horra, R., and Arche, A.: A comparison of the Iberian and Ebro Basins during the Permian and Triassic, eastern Spain: A quantitative subsidence modelling approach, *Tectonophysics*, 474, 160–183, <https://doi.org/10.1016/j.tecto.2008.06.005>, 2009.
- Vergés, J. and Fernández, M.: Tethys–Atlantic interaction along the Iberia–Africa plate boundary: The Betic–Rif orogenic system, *Tectonophysics*, 579, 144–172, <https://doi.org/10.1016/j.tecto.2012.08.032>, 2012.
- Vergés, J. and Sàbat, F.: Constraints on the Neogene Mediterranean kinematic evolution along a 1000 km transect from Iberia to Africa, in: *Geological Society, London, Special Publications*, 63–80, <https://doi.org/10.1144/GSL.SP.1999.156.01.05>, 1999.
- Wells, D. L. and Coppersmith, K. J.: New empirical relationships among magnitude, rupture length, rupture width, rupture area, and surface displacement, *B. Seismol. Soc. Am.*, 84, 974–1002, <https://doi.org/10.1785/BSSA0840040974>, 1994.
- Weng, H. and Yang, H.: Seismogenic width controls aspect ratios of earthquake ruptures, *Geophys. Res. Lett.*, 44, 2725–2732, <https://doi.org/10.1002/2016GL072168>, 2017.
- Withjack, M. O. and Callaway, S.: Active normal faulting beneath a salt layer; an experimental study of deformation patterns in the cover sequence, *AAPG Bull.*, 84, 627–651, <https://doi.org/10.1306/C9EBCE73-1735-11D7-8645000102C1865D>, 2000.
- Withjack, M. O., Olson, J., and Peterson, E.: Experimental models of extensional forced folds, *AAPG Bull.*, 74, 1038–1054, <https://doi.org/10.1306/0C9B23FD-1710-11D7-8645000102C1865D>, 1990.
- Yen, Y. and Ma, K.: Source-scaling relationship for M 4.6–8.9 earthquakes, specifically for earthquakes in the collision zone of Taiwan, *B. Seismol. Soc. Am.*, 101, 464–481, <https://doi.org/10.1785/0120100046>, 2011.